




RESEARCH ARTICLE

Astrocyte structural heterogeneity in the mouse hippocampus

João Filipe Viana^{1,2} | João Luís Machado^{1,2} | Daniela Sofia Abreu^{1,2} |
 Alexandra Veiga^{1,2} | Sara Barsanti^{1,2} | Gabriela Tavares^{1,2} | Manuella Martins^{1,2} |
 Vanessa Morais Sardinha^{1,2} | Sónia Guerra-Gomes^{1,2} | Cátia Domingos³ |
 Alberto Pauletti³ | Jérôme Wahis⁴ | Chen Liu⁴ | Corrado Cali^{5,6}  |
 Christian Henneberger^{3,7}  | Matthew G. Holt^{4,8}  | João Filipe Oliveira^{1,2,9} 

¹Life and Health Sciences Research Institute (ICVS), School of Medicine, University of Minho, 4710-057 Braga, Portugal

²ICVS/3B's - PT Government Associate Laboratory, Braga, Portugal

³Institute of Cellular Neurosciences, Medical Faculty, University of Bonn, Bonn, Germany

⁴Laboratory of Glia Biology, VIB-KU Leuven Center for Brain and Disease Research, Leuven, Belgium

⁵Department of Neuroscience, University of Torino, Torino, Italy

⁶NICO - Neuroscience Institute Cavalieri Ottolenghi, Orbassano, Italy

⁷German Center for Neurodegenerative Diseases (DZNE), Bonn, Germany

⁸Synapse Biology Group, Instituto de Investigação e Inovação em Saúde (i3S), University of Porto, 4200-135 Porto, Portugal

⁹IPCA-EST-2Ai, Polytechnic Institute of Cávado and Ave, Applied Artificial Intelligence Laboratory, Campus of IPCA, Barcelos, Portugal

Correspondence

João Filipe Oliveira, Life and Health Sciences Research Institute (ICVS) - School of Medicine, University of Minho, Campus de Gualtar, 4710-057 Braga, Portugal.

Email: joaooliveira@med.uminho.pt

Funding information

Foundation for Science and Technology (FCT), Grant/Award Numbers: UIDP/50026/2020, UIDB/50026/2020; IF grant, Grant/Award Number: IF/00328/2015; Bial Foundation, Grant/Award Number: 037/18; "la Caixa" Foundation, Grant/Award Number: LCF/PR/HR21/52410024; Portuguese Platform of Bioimaging, Grant/Award Number: PPBI-POCI-01-0145-FEDER-022122; German Research Foundation, Grant/Award Numbers: HE6949/3, SPP1757 HE6949/1, SFB1089 B03; European Union, Grant/Award Number: H2020-MSCA-ITN; Fonds Wetenschappelijk Onderzoek, Grant/Award Number: G066715N; KU Leuven Internal Funding (C1 grant), Grant/Award Number: C14/20/071; European Research Council (ERC) Grant, Grant/Award Number: 281961;

Abstract

Astrocytes are integral components of brain circuits, where they sense, process, and respond to surrounding activity, maintaining homeostasis and regulating synaptic transmission, the sum of which results in behavior modulation. These interactions are possible due to their complex morphology, composed of a tree-like structure of processes to cover defined territories ramifying in a mesh-like system of fine leaflets unresolved by conventional optic microscopy. While recent reports devoted more attention to leaflets and their dynamic interactions with synapses, our knowledge about the tree-like "backbone" structure in physiological conditions is incomplete. Recent transcriptomic studies described astrocyte molecular diversity, suggesting structural heterogeneity in regions such as the hippocampus, which is crucial for cognitive and emotional behaviors. In this study, we carried out the structural analysis of astrocytes across the hippocampal subfields of *Cornu Ammonis* area 1 (CA1) and dentate gyrus in the dorsoventral axis. We found that astrocytes display heterogeneity across the hippocampal subfields, which is conserved along the dorsoventral axis. We further found that astrocytes appear to contribute in an exocytosis-dependent manner to a signaling loop that maintains the backbone structure. These findings reveal

João Filipe Viana and João Luís Machado contributed equally to this study.

This is an open access article under the terms of the [Creative Commons Attribution-NonCommercial-NoDerivs](https://creativecommons.org/licenses/by-nc-nd/4.0/) License, which permits use and distribution in any medium, provided the original work is properly cited, the use is non-commercial and no modifications or adaptations are made.

© 2023 The Authors. GLIA published by Wiley Periodicals LLC.

European Commission, Grant/Award Numbers: 951923, H2020-WIDESPREAD-2018-2020-6; FWO post-doctoral fellowships, Grant/Award Numbers: 1513020N, 12V7522N, 12V7519N

astrocyte heterogeneity in the hippocampus, which appears to follow layer-specific cues and depend on the neuro-glial environment.

KEYWORDS

astrocyte, dorsal, hippocampus, morphology, skeleton, ventral

1 | INTRODUCTION

Astrocytes are ubiquitous cells in the mammalian central nervous system that display a highly ramified morphology (Bushong et al., 2002; Cali et al., 2019; Emsley & Macklis, 2006; Endo et al., 2022; Khakh & Sofroniew, 2015; Livet et al., 2007; Refaeli et al., 2021; Torres-Ceja & Olsen, 2022; Wilhelmsson et al., 2006). This feature allows them to maintain homeostatic and synaptic regulation through close contact and dynamic interactions with neurons, other glia, blood vessels, and extracellular matrix, ultimately modulating brain circuit function with an impact on behavior (Araque et al., 2014; de Oliveira Figueiredo et al., 2022; Hirrlinger & Nimmerjahn, 2022; Nagai et al., 2020; Oliveira et al., 2015; Oliveira & Araque, 2022; Rusakov et al., 2014).

Astrocytic morphology displays at least two levels of complexity (Arizono & Nägerl, 2022; Khakh & Sofroniew, 2015; Torres-Ceja & Olsen, 2022). The first level consists of a tree-like structure, referred to here as “backbone,” including main processes originating in the soma and several orders of ramification into branchlets and end-feet. The backbone structure is rich in intermediate filaments such as glial fibrillary acidic protein (GFAP) and microtubule proteins. The size of these structures is in the micrometer range and may be visualized using conventional microscopy (Chai et al., 2017; Eilam et al., 2016; Endo et al., 2022; Grosche et al., 2013; Jones et al., 2018; Karpf et al., 2022; Refaeli et al., 2021; Xu et al., 2014). This structure ramifies to a second level consisting of a mesh-like network of leaflets that includes perisynaptic processes (PAPs) and end-feet. Leaflets are mainly composed of actin filaments and display activity-dependent motility. The size of these structures is often below the diffraction limit of conventional light microscopy, requiring more sophisticated techniques to study them (e.g., electron, super-resolution or expansion microscopy or volume fraction analysis) (Arizono et al., 2021; Aten et al., 2022; Cali et al., 2019; Minge et al., 2021; Salmon et al., 2023; Zisis et al., 2021).

While recent literature studying astrocyte morphology devoted more attention to leaflets and their dynamic interactions with synapses (Bernardinelli et al., 2014; Genoud et al., 2006; Henneberger et al., 2020; Herde et al., 2020; Lavalie et al., 2011; Lushnikova et al., 2009), our knowledge about the tree-like backbone structure in physiological conditions remains simplistic. The recent finding that leaflets appear to differentially stem from every astrocytic region (soma, primary processes/branches, and branchlets) (Aten et al., 2022) raised the importance of the properties of astrocytic scaffold that extends to an extensive territory, up to tens of micrometers in the rodent and 2–3 fold more complex in the human brain (Bushong et al., 2002; Livet et al., 2007; Oberheim et al., 2009; Refaeli

et al., 2021; Wilhelmsson et al., 2006). Moreover, recent transcriptomic studies described different astrocytic profiles and suggested structural heterogeneity of astrocytes across brain regions (Endo et al., 2022) and within brain regions such as the hippocampus and the cortex (Batiuk et al., 2020; Bayraktar et al., 2020; Karpf et al., 2022). Indeed, a recent study reported that astrocytes in the somatosensory cortex display distinct territorial volume and arborization across the cortical layers (Lanjakornsiripan et al., 2018). Morphological heterogeneity appears as a hallmark of complex brain circuits correlating, for instance, with the functional properties of astrocytic networks (Anders et al., 2014). However, the evidence regarding structural heterogeneity across the hippocampus, a brain region crucial for cognitive and emotional processing (Oliveira et al., 2015; Santello et al., 2019), is still scarce. Astrocyte-neuron interactions in this region were shown to underlie behavior modulation (Adamsky et al., 2018; Navarrete et al., 2019; Sardinha et al., 2017), reinforcing the need to understand better molecular and structural heterogeneity of astrocytes in this region.

To assess astrocyte hippocampal structural heterogeneity, we carried out the tridimensional reconstruction of astrocytes across the hippocampal subfields of *Cornu Ammonis* area 1 (CA1) and dentate gyrus (DG) in the dorsoventral axis. We found that astrocytes display considerable heterogeneity across the hippocampus subfields, which is conserved along the dorsoventral axis. Astrocytes appear to contribute with an exocytosis-dependent signaling loop to the self-maintenance of the backbone structure.

2 | METHODS

2.1 | Animals

All procedures involving mice were performed according to the guidelines for the welfare of laboratory mice as described in Directive 2010/63/EU. In addition, they were approved by the Local Ethics Committee (ORBEA 004/2018) and the National Authority for Animal Experimentation, DGAV (DGAV 023838). Male mice 10–16 week-old were group-housed in standard cages (3–6 mice per cage) with food and water *ad libitum*. The housing room was at 22°C with controlled ventilation and under a light/dark cycle of 12 h (lights on from 8 a.m. to 8 p.m.). To assess the morphology of astrocytes in the CA1 and DG sub-regions of the dorsal and ventral hippocampus, coronal brain slices were obtained from (i) C57BL/6J mice ($N = 9$); (ii) mice expressing the EGFP-labeled Rpl10a ribosomal subunit specifically in astrocytes (hereafter referred to as “AstroTRAP” mice; $N = 2$). These

mice were obtained by crossing Rosa26fsTRAP (Zhou et al., 2013) and astrocyte-specific *Fgfr3-iCreER^{T2}* mice (Young et al., 2010). Final EGFP-Rpl10a expression in astrocytes was induced by intraperitoneal injection of tamoxifen (MP Biomedicals, 156738) (75 mg/kg dissolved in corn oil) once a day for 5 days. Genotyping of all mouse lines was performed using PCR using published primers. Rosa26fsTRAP were initially obtained from Jackson Laboratory (Strain #022367), whereas *Fgfr3-iCreER^{T2}* mice were obtained from William D. Richardson (University College London) under an MTA. AstroTRAP mice display EGFP-labeled ribosomes in the cytosol, allowing a detailed morphological visualization (Sakers et al., 2017); and (iii) mice expressing EGFP in astrocytes under the GFAP promoter (Nolte et al., 2001) for the analysis of the astrocyte volume fraction and territory ($N = 20$). To assess the modulatory effect of astrocytic exocytosis on astrocyte morphology, we obtained coronal brain slices from the dominant-negative SNARE (dnSNARE) mouse model (Pascual et al., 2005). Wild-type (WT) littermates ($N = 5$) and dnSNARE mice ($N = 5$) were bred as described previously, and doxycycline (100 µg/mL) was removed from the drinking water 6 weeks before the experiment (Sardinha et al., 2017). To assess the role of D-serine in the rescue of astrocytic structure, D-serine was administered as previously described (Sardinha et al., 2017) for four consecutive days (Sigma-Aldrich, United States; 1 g/kg of body weight, 10 mL/kg of body weight in saline, i.p.) to a new set of WT ($N = 2$) and dnSNARE ($N = 3$) mice. Control mice of both genotypes received similar saline administration: WT ($N = 2$) and dnSNARE ($N = 3$) mice. This administration was described to increase the intracerebral levels of D-serine and rescue functional deficits in different contexts and independent laboratories (Guercio et al., 2014; Han et al., 2015).

2.2 | Tissue processing

C57BL/6J, dnSNARE, and respective littermate WT mice were deeply anesthetized with a mixture of ketamine and medetomidine, followed by intracardiac perfusion with saline and 4% paraformaldehyde (PFA). Brains were carefully removed and immersed in 4% PFA for 36 h at room temperature (RT) and then transferred to a 30% sucrose solution at 4°C until sinking. After impregnation with sucrose, brains from C57BL/6J mice were immersed in a 3% agarose solution and sectioned using a vibratome (thickness: 50 µm; Leica VT1000S, Germany). Brain slices were maintained in phosphate-buffered saline (PBS) solution until the immunolabeling protocol. Brains from dnSNARE and respective WT mice were cryopreserved in Neg-50 medium (ThermoFisher Scientific, United States) at −20°C until sectioning in a cryostat (thickness: 20 µm; Leica CM1900, Germany). Brain slices were thawed and dried, at RT, for 10 min before the immunolabeling protocol.

Brain slices were washed in PBS solution followed by permeabilization with 0.3% Triton-X100 (Sigma Aldrich, United States) in PBS solution (0.3% PBS-T) for 10 min. After permeabilization, the tissue from dnSNARE and WT mice was submitted to an antigen retrieval step with citrate buffer (10 mM, pH 6.0, Sigma-Aldrich). Briefly, slices

were placed in a preheated citrate solution and incubated two times for 10 min at 100 W microwave potency and then left to cool for 15 min. Then the slices were washed in PBS and incubated with the blocking solution of normal goat serum (NGS; 10%) in PBS for C57BL/6J mice, or fetal bovine serum (FBS; 10%) in PBS for dnSNARE mice for 1 h at RT. This blocking step was followed by overnight incubation, at 4°C, with the primary antibodies rabbit polyclonal anti-GFAP (1:200; Dako, Denmark) and/or goat polyclonal anti-GFP (1:300; Abcam, United Kingdom) in a 0.3% PBS-T solution with 2% NGS/FBS. On the next day, the slices were washed in PBS and incubated with the secondary antibody Alexa Fluor® 594 goat anti-rabbit (1:1000; Invitrogen, ThermoFisher Scientific, United States) and/or Alexa Fluor® 488 donkey anti-goat (1:1000; Invitrogen, ThermoFisher Scientific, United States), in a 0.3% PBS-T solution with 2% NGS/FBS, for 1 h at RT. After incubation, the slices were rinsed with PBS, and the nuclei were labeled for 10 min at RT with 4',6-diamidino-2-phenylindole (DAPI, 1:1000; Invitrogen, United States). Finally, slices were washed with PBS and mounted using Immumount (ThermoFisher Scientific, United States). All procedures during this day were performed in the dark.

Brains from AstroTRAP mice were processed as follows: 14 days post-tamoxifen administration, mice were trans-cardially perfused with PBS followed by 4% PFA in PBS. Brains were extracted and post-fixed in 4% PFA in PBS at 4°C for 24 h, and coronally sectioned (thickness: 50 µm; Leica VT1000S, Germany). Sections were then blocked with 10% Normal Donkey Serum (NDS, Abcam) and 0.2% Triton X-100 (Sigma-Aldrich) in Tris-buffered saline (TBS) for 3 h at RT. Sections were then incubated overnight at 4°C in a TBS-based primary antibody solution, composed of 10% NDS, 0.2% Triton X-100, and chicken anti-EGFP antibody (1:500 dilution, Aves Labs, GFP-1010). Following 6 × 10 min washes in TBS, sections were then incubated for 3 h at RT in a TBS-based secondary antibody solution, composed of 2.5% NDS, 0.2% Triton X-100, donkey anti-chicken Alexa 488 antibody (1:200 dilution, Jackson ImmunoResearch, 703-545-155). Following 6 × 10 min washes in TBS, sections were mounted onto Superfrost slides (ThermoFisher Scientific) and coverslipped in Fluoromount-G medium with DAPI (ThermoFisher Scientific).

Brain slices were imaged on an Olympus LPS FV1000 confocal microscope (Olympus, Germany) using the 20× (N.A. 0.70; 1.5 µm of z-step; 1024 × 1024 pixels) and the 60× (N.A. 1.42; 1.0 µm of z-step; 640 × 640 pixels) objectives. The images from the CA1 and DG regions of the hippocampus were obtained following the coordinates of the mouse brain atlas (Paxinos & Franklin, 2001): dorsal hippocampus, 1.8 ± 0.1 mm posterior to bregma; ventral hippocampus, 3.4 ± 0.1 mm posterior to bregma. The brain tissue for each experiment was processed (sectioned, stored, and stained) simultaneously to minimize staining heterogeneity between samples. Slight staining differences might be found between figures, considered independent experiments. As astrocyte reconstructions were performed based on the GFAP or GFP immunolabeling, the penetration and equal distribution of antibodies in the whole depth of the tissue should be guaranteed. Based on previous reports and our own experience, the slice

thickness used in each figure secured the visualization of GFAP structure across the tissue depth. Moreover, the analysis of backbone structure in thinner brain slices should consider the truncation of astrocyte processes. Therefore, in each experiment, the comparisons are performed between groups whose data was obtained using the same experimental conditions.

2.3 | Tridimensional reconstruction of astrocytic backbone

The tridimensional (3D) reconstruction of the astrocytic backbone was performed in the following subfields of the hippocampus: CA1 (*stratum oriens*, *stratum radiatum*, and *stratum lacunosum moleculare*) and DG (*stratum moleculare* and hilus). In confocal z-stacks obtained from C57BL/6J, dnSNARE, and respective WT mice, we skeletonized the GFAP-stained structure. In confocal z-stacks from AstroTRAP mice, we skeletonized astrocytes based on EGFP expression. We used a semi-automatic tool called SNT, an updated version of the Simple Neurite Tracer, a free Fiji-ImageJ software plugin (<http://fiji.sc/Fiji>). We previously validated this tool to quantify different features of astrocytic structure: total process length, number of processes, complexity of the astrocytic arbor given by Sholl analysis, and the last process intersection given by the maximum intersection radius in the Sholl analysis, as a fiduciary marker to outline limits of the cell (Tavares et al., 2017). Briefly, the reconstruction of the selected astrocytes began by marking the center of the DAPI-stained nucleus, around which every primary process originates. Next, a distant point within the primary process was selected, and SNT automatically determined the process midline and tortuosity. After confirming the suggested path, this step was repeated until the primary process, respective branches, and branchlets were reconstructed entirely. This process was repeated for every primary process until the complete reconstruction of the astrocyte. Representative 3D astrocyte skeletons provided in the figures were exported to .SVG format using SNT > Utilities > Reconstruction Plotter. In each figure, the 3D skeletons illustrated were selected from astrocytes displaying a total process length and number of processes closest to the group mean. We reconstructed a maximum of four astrocytes per z-stack and an equal number of z-stacks per animal.

2.4 | Volume fraction and territory analyses

The astrocyte volume fraction and territory size from astrocytes in acute hippocampal slices were calculated as described in detail previously (Anders et al., 2014; Minge et al., 2021). Briefly, acute hippocampal slices (thickness 300 μm) were prepared from mice expressing EGFP in astrocytes (Nolte et al., 2001). Images of EGFP-expressing astrocytes were taken using two-photon excitation fluorescence microscopy (10–11 images per animal). Please see Anders et al. (2014) and Minge et al. (2021) for a detailed description of the slice preparation and imaging procedures. Single horizontal cross-sections of

astrocytes taken through their cell bodies were obtained from the various subregions. We have previously shown that analyses of single subsections are representative of the entire astrocyte and particularly useful for the analyses of large cell populations (Minge et al., 2021). We analyzed the area of the astrocyte cross-section as a measure of its territory size and the astrocyte volume fraction as an indicator of astrocyte cell volume.

2.5 | Astrocyte density

The density of astrocytes was determined in z-projections of confocal image stacks (20 \times magnification) obtained from C57BL/6J mice ($N = 6$) in the layers of the dorsal and ventral hippocampus analyzed for Figures 1 and 3. The plugin “Cell Counter” in FIJI was used to quantify GFAP-positive cells. The layer under study was delimited following coordinates published in the mouse brain atlas (Paxinos & Franklin, 2001) and measured. Only cells that presented GFAP-staining co-localized with DAPI staining were included. The volume of tissue analyzed was given by the product of the area analyzed multiplied by the respective number of z-stack images (1 μm inter-image interval). GFAP-positive astrocyte densities were normalized per $10^6 \mu\text{m}^3$. Data are presented as the average of 2–3 z-stacks per animal.

2.6 | Statistical analysis

Statistical analysis was performed using GraphPad Prism version 8 (GraphPad Software, La Jolla CA, United States). Most datasets, including continuous measures, passed the Shapiro–Wilk normality test for normal distribution. Analysis of astrocytic total process length, number of processes and density of astrocytes across different hippocampal layers and effect of EGFP expression in the dnSNARE experiment was performed by a one-way analysis of variance (ANOVA), followed by Tukey's multiple comparisons test. Student's t test was used to compare WT versus dnSNARE parameters. For Sholl analysis and D-serine treatment, a two-way ANOVA and Tukey's or Sidak's multiple comparison test was applied. The values are presented as mean \pm standard error of the mean (SEM). Measures of volume fraction and last intersection failed to pass the normality test and were compared by the Kruskal–Wallis test. Significant statistical differences were considered when $p \leq .05$.

3 | RESULTS

3.1 | Astrocytes display backbone heterogeneity across the layers of the dorsal hippocampus

Astrocytic backbone heterogeneity was first assessed by skeletonization of the GFAP-immunolabeled structure in different layers of the dorsal hippocampus. The reconstruction was performed in confocal z-stacks

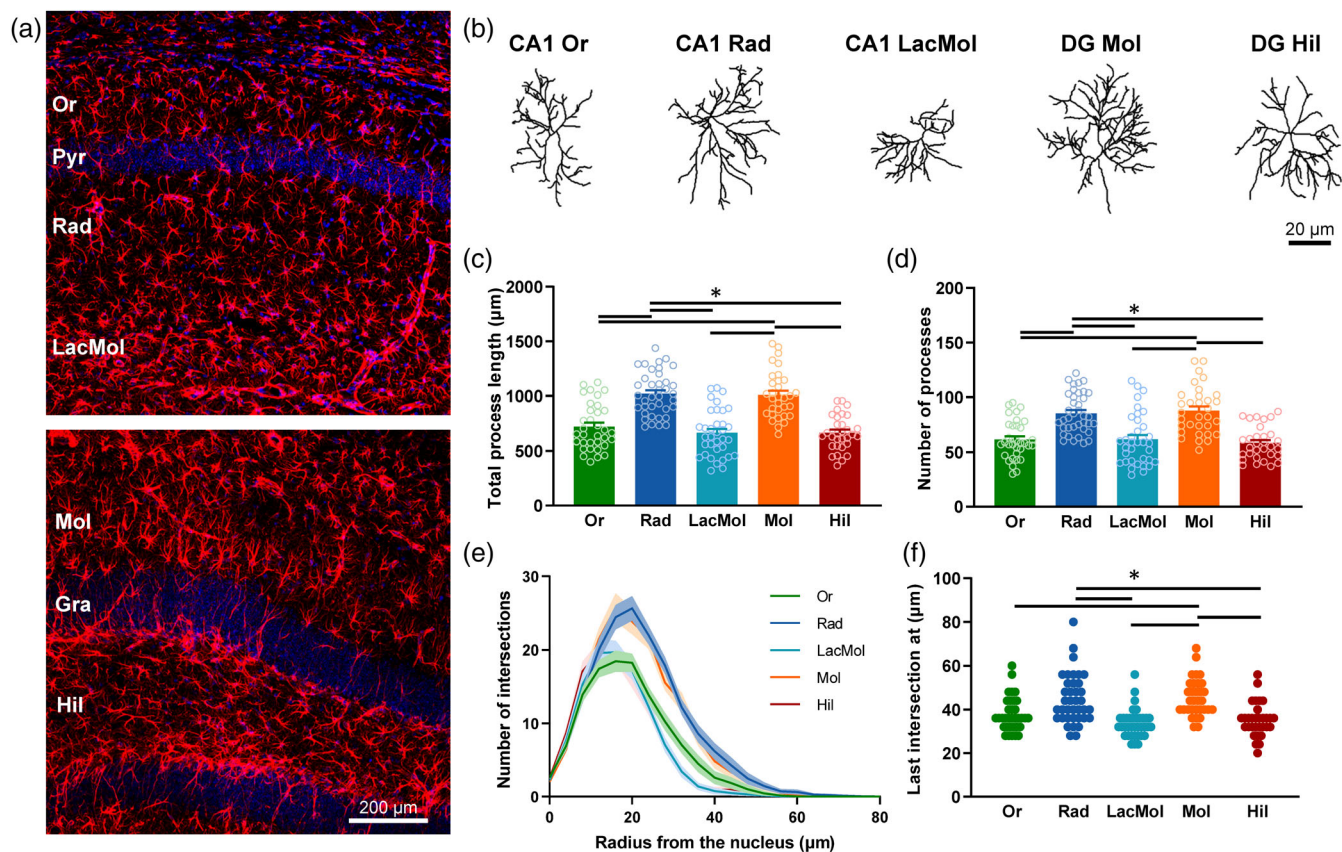


FIGURE 1 Astrocytes display backbone heterogeneity across the layers of the dorsal hippocampus. (a) Maximum projection of confocal image z-stacks of GFAP-immunolabeled astrocytes (red) in the CA1 (top) *stratum oriens* (Or), *stratum radiatum* (Rad), *stratum lacunosum moleculare* (LacMol) and DG (bottom) *stratum moleculare* (Mol) and hilus (Hil); (b) representative 3D reconstruction of astrocytes from Or, Rad, LacMol, Mol and Hil layers; characterization of astrocyte 3D structures by analysis of (c) total process length, (d) number of processes, (e) Sholl analysis and (f) last intersection radius. Data plotted as individual astrocyte values (dots) and mean \pm SEM (columns and bars). Number of cells/group: 34, 38, 35, 32, 31 in $N = 4$ mice. * $p \leq .05$.

acquired from the CA1 and DG subfields, including: CA1 *stratum oriens* (Or), *stratum radiatum* (Rad), and *stratum lacunosum moleculare* (LacMol); DG *stratum moleculare* (Mol), and hilus (Hil) (Figure 1a). This analysis revealed heterogeneity of the astrocyte backbone in terms of total process length, number of processes, and arbor complexity given by Sholl analysis (Figure 1b–f; descriptive statistics in Table S1). Specifically, *post-hoc* tests revealed that CA1 Rad astrocytes displayed a longer process length when compared to astrocytes of CA1 Or ($p < .001$), CA1 LacMol ($p < .001$), and DG Hil ($p < .001$) (Figure 1c). In addition, DG Mol astrocytes displayed a longer total process length than those of CA1 Or ($p < .001$), CA1 LacMol ($p < .001$), and DG Hil ($p < .001$) (Figure 1c). In line with this, CA1 Rad astrocytes also presented a higher number of processes than astrocytes of the CA1 Or ($p < .001$), CA1 LacMol ($p < .001$), and DG Hil ($p < .001$) (Figure 1d). Similarly, DG Mol astrocytes presented a higher number of processes than astrocytes of the CA1 Or ($p < .001$), CA1 LacMol ($p < .001$), and DG Hil ($p < .001$). The Sholl analysis confirmed that astrocytes in the five layers of CA1 and DG display a typical tree-like structure with an increasing number of intersections until 12–16 μm distance from the nucleus, followed by a steady decrease (Figure 1e). Two-way ANOVA *post-hoc* analysis confirmed the higher complexity of astrocyte arbors in the CA1 Rad and

DG Mol (statistical details in Table S2). Finally, the distance from the soma to the last process intersection was longer for astrocytes in the CA1 Rad (than CA1 LacMol, $p < .001$; DG Hil $p = .001$) and DG Mol (than CA1 Or, $p = .005$; CA1 LacMol $p < .001$; DG Hil $p < .001$) (Figure 1f), suggesting that these astrocytes occupy larger territories. In summary, the GFAP-stained backbone of astrocytes in the dorsal hippocampus is heterogeneous, as astrocytes of the CA1 Rad and DG Mol display more complex arbors.

To validate the data obtained from tissue stained with anti-GFAP antibodies, a similar analysis was performed using brain tissue from AstroTRAP mice, which also allowed the reconstruction of different astrocyte populations in the CA1 and DG layers (Figure 2a), albeit this approach enabled a more extensive visualization of astrocyte morphology due to the distribution of EGFP-tagged ribosomes in the cytosol, compared to GFAP staining, which is purely cytoskeletal. Results in the AstroTRAP model confirmed the structural heterogeneity observed with anti-GFAP staining, as astrocytes from the CA1 Rad and DG Mol display more complex arbors (Figure 2b–f; descriptive statistics in Table S1). Specifically, astrocytes from the CA1 Rad and DG Mol show longer process length than astrocytes from the CA1 Or ($p < .001$), CA1 LacMol ($p < .001$), and DG Hil ($p < .001$) (Figure 2c). Likewise, CA1 Rad

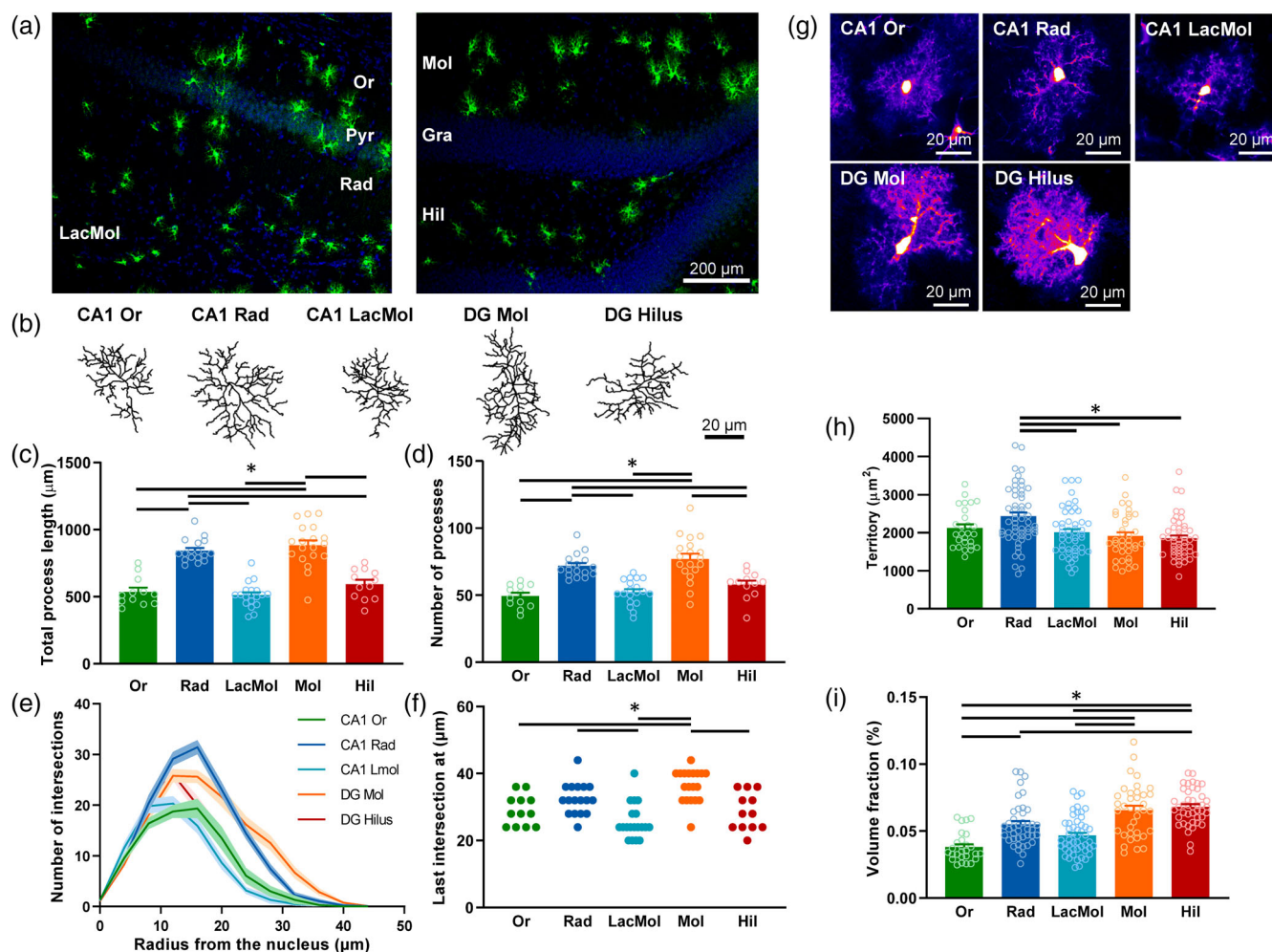


FIGURE 2 Astrocytic backbone heterogeneity in the dorsal hippocampus is maintained in complementary preparations. (a) Maximum projection of confocal image z-stacks of astrocytes in AstroTRAP mouse tissue containing the CA1 (left) *stratum oriens* (Or), *stratum radiatum* (Rad), *stratum lacunosum moleculare* (LacMol) and DG (right) *stratum moleculare* (Mol) and hilus (Hil) immunolabeled against EGFP (green); (b) representative 3D reconstruction of astrocytes from Or, Rad, LacMol, Mol and Hil layers; characterization of astrocyte 3D structures by analysis of (c) total process length, (d) number of processes, (e) Sholl analysis and (f) last intersection radius. (g) Representative images of EGFP-expressing astrocytes in the five subregions. (h) Astrocyte territory and (i) volume fraction excluding the soma; data plotted as individual astrocyte values (dots) and mean \pm SEM (columns and bars). Number of cells/group: (c–f), 12, 17, 19, 19, 12 in $N = 2$ mice; (h): 27, 55, 50, 37, 48 cells; (i): 27, 41, 50, 37, 43 cells in $N = 20$ mice. * $p \leq .05$.

and DG Mol astrocytes have more processes than CA1 Or ($p < .001$), CA1 LacMol ($p < .001$), and DG Hil (Rad, $p = .017$; Mol, $p < .001$) astrocytes (Figure 2d). Regarding arbor complexity, in this preparation, hippocampal astrocytes display the same increase in their complexity until 12–16 μm from the soma, following a decrease from this point onwards. Further two-way ANOVA post hoc analysis confirmed that astrocytes from the CA1 Rad and DG Mol are more complex, generally displaying more process intersections at similar radial distances from the soma (Figure 2e; statistical details in Table S2). Finally, measurements of the radial distance of the last process intersection also suggest that astrocytes occupy larger territories in the CA1 Rad (than CA1 LacMol, $p = .010$) and in the DG Mol (than CA1 Or, $p = .014$; CA1 LacMol, $p < .001$; and DG Hil, $p = .010$) (Figure 2f). In summary, this alternative experimental protocol allowed the reconstruction of the astrocytic structure based on the distribution of EGFP-tagged ribosomes in the

cytosol. It also confirmed that different populations of astrocytes in the CA1 Rad and DG Mol display a more complex structure than astrocytes in the other hippocampal layers.

Finally, to assess the overall morphological parameters of an entire astrocyte, we also analyzed territory size (i.e., cross-section areas) and the fraction of tissue volume occupied by astrocytes within these territories (Figure 2g–i). As described and verified previously (Minge et al., 2021), this analysis captures morphological features of entire astrocytes, including fine astrocytic processes below the diffraction limit of conventional microscopy. This alternative method indicates that astrocytes of the CA1 Rad display a larger cross-sectional area than astrocytes of CA1 LacMol ($p = .006$), DG Mol ($p = .001$), and DG Hil, ($p < .001$) (Figure 2h). This result suggests that they occupy a larger territory, which is in line with the observations using both anti-GFAP staining and GFP imaging in tissue from

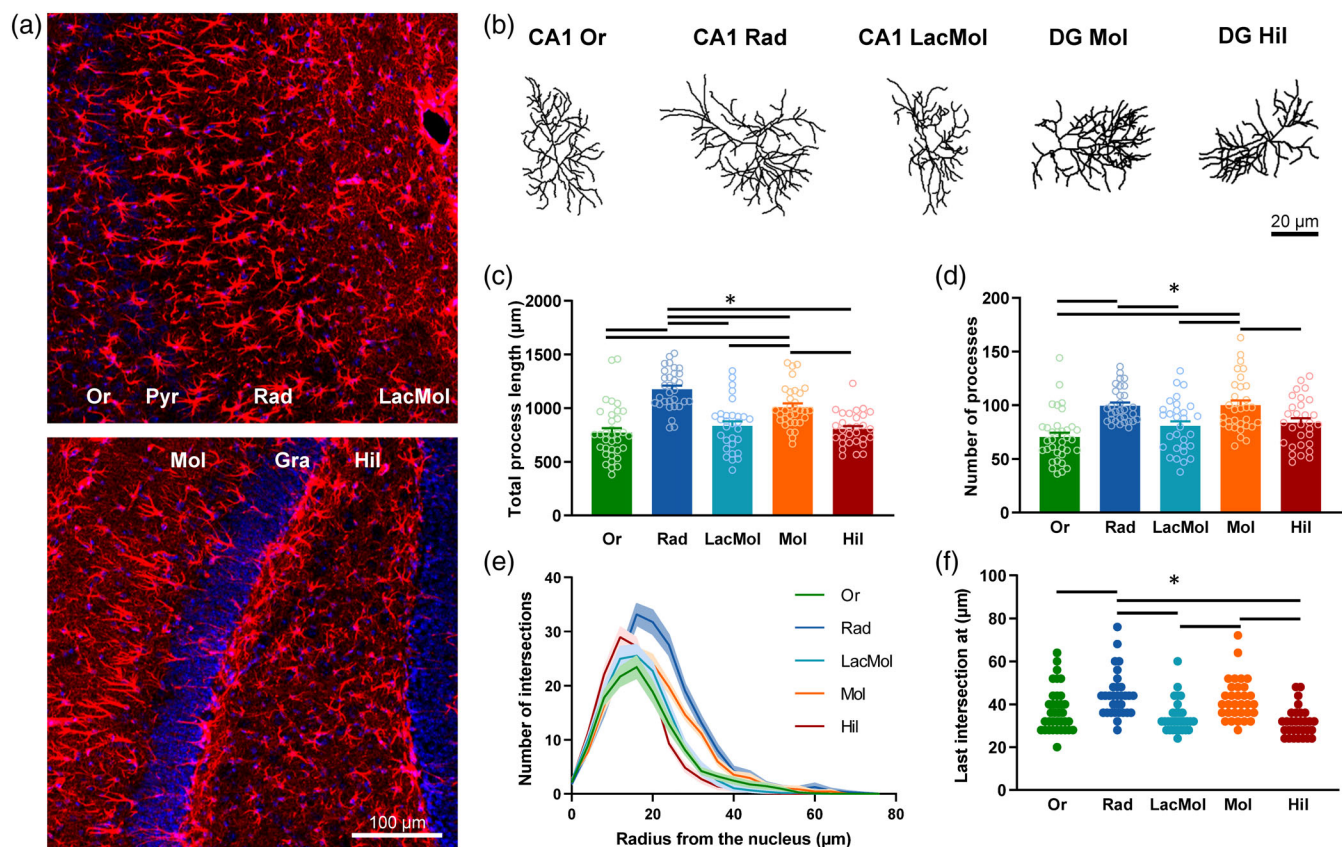


FIGURE 3 Astrocytic backbone heterogeneity is maintained across the layers of the ventral hippocampus. (a) Maximum projection of confocal image z-stacks of GFAP-immunolabeled astrocytes (red) in the CA1 (top) *stratum oriens* (Or), *stratum radiatum* (Rad), *stratum lacunosum moleculare* (LacMol) and DG (bottom) *stratum moleculare* (Mol) and hilus (Hil) immunolabeled with anti-GFAP antibodies (red); (b) representative 3D reconstructions of astrocytes from Or, Rad, LacMol, Mol and Hil layers; characterization of astrocyte 3D structures by analysis of (c) total process length, (d) number of processes, (e) Sholl analysis, and (f) last intersection radius. Data plotted as individual astrocyte values (dots) and mean \pm SEM (columns and bars). Number of cells/group: 35, 31, 30, 32, 30 in $N = 4$ mice. $*p \leq .05$.

AstroTRAP mice. Moreover, based on the fraction of tissue volume occupied (Figure 2i), astrocytes in the CA1 Rad, DG Mol, and DG Hil appear to occupy a higher percentage of tissue volume in their territories than in the other layers (Rad-Or, $p = .001$; Mol-Or, $p < .001$; Mol-LacMol, $p < .001$; Hil-Or, $p < .001$; Hil-Rad, $p = .005$; Hil-LacMol, $p < .001$). Together these findings suggest that morphological heterogeneity occurs independently on different morphological levels (backbone vs. leaflets) across the five regions.

Our findings document astrocyte heterogeneity across the layers of the dorsal hippocampus, where CA1 Rad and DG Mol astrocytes display a larger and more complex backbone. Moreover, the validation of the results by different methodological approaches confirms that 3D skeletonizing of anti-GFAP immunostaining is a feasible and reliable approach to screen astrocyte backbone complexity.

3.2 | Astrocyte backbone heterogeneity is conserved along the dorsoventral axis

To assess whether the structural heterogeneity observed in the dorsal hippocampus is maintained along the dorsoventral axis, skeletons of

anti-GFAP immunostained astrocytes were obtained in the corresponding layers of the CA1 and DG subfields of the ventral hippocampus (Figure 3a). Similar to what was observed in the dorsal hippocampus, astrocytes from the CA1 and DG subfields of the ventral hippocampus present heterogeneous backbone complexity, as shown by the total process length, number of processes, and arbor complexity (Figure 3b-f; descriptive statistics in Table S1). Specifically, CA1 Rad astrocytes display a longer process length than astrocytes from the CA1 Or ($p < .001$), CA1 LacMol ($p < .001$), DG Mol ($p = .015$) and DG Hil ($p < .001$). Likewise, astrocytes from the DG Mol possess a longer total process length than astrocytes from the CA1 Or ($p < .001$), CA1 LacMol ($p = .010$), and DG Hil ($p = .002$) (Figure 3c). Regarding the number of processes, astrocytes from the CA1 Rad possess more processes than astrocytes from the CA1 Or ($p < .001$) and CA1 LacMol ($p = .012$). As expected, astrocytes from the DG Mol also possess more processes than astrocytes from the CA1 Or ($p < .001$), CA1 LacMol ($p = .009$), and DG Hil ($p = .044$) (Figure 3d). Furthermore, Sholl analysis showed that CA1 Rad and DG Mol astrocytes display more complex arbors than astrocytes in the remaining layers (Figure 3e; statistical details in Table S2). In line with this, astrocytes from the CA1 Rad and DG Mol presented a higher



radial distance from the soma to the last intersection than astrocytes from CA1 Or (to Rad, $p = .018$), CA1 LacMol (to Rad, $p < .001$; to Mol, $p = .003$) and DG Hil (to Rad, $p < .001$; to Mol, $p < .001$) (Figure 3f). Thus, as in the dorsal hippocampus, CA1 Rad and DG Mol astrocytes in the ventral hippocampus are more complex and have a higher total process length and number of processes than their counterparts in CA1 Or, CA1 LacMol, and DG Hil.

The comparison of astrocyte structures in the same layers along the dorsal and ventral axes showed that astrocytes in the ventral hippocampus are more complex than in the corresponding layer in the dorsal field (Figure S1a). This is the case for most layers studied in terms of the total process length (CA1 Rad, $p = .009$; CA1 LacMol, $p = .004$; and the DG Hil, $p = .033$; Figure S1b) and the number of processes (CA1 Rad, $p = .026$; CA1 LacMol, $p = .001$; and the DG Hil, $p < .001$; Figure S1c). This is translated into increased arbor complexity for all layers, except in the DG Mol (Figure S1d; statistical details in Table S2). Curiously, despite these larger arbors, astrocytes do not occupy larger territories (Figure S1e). In summary, astrocytes in the ventral hippocampus (except for the DG Mol) are more ramified, while occupying virtually similar territories.

Interestingly, in all layers analyzed in the dorsal and ventral regions of the hippocampus, no apparent overlap of astrocytes backbones was observed, suggesting that the non-overlapping (tiled) astrocytic territories described previously in CA1 Rad (Bushong et al., 2002; Livet et al., 2007; Wilhelmsson et al., 2006) are maintained across the subfields of the hippocampus, along the dorsoventral axis. Based on these observations, it would be expected that layers containing astrocytes displaying more complex structures could display lower cell density. The opposite would also be expected to maintain territorial coverage of the whole tissue volume. To assess this hypothesis, we assessed astrocyte densities in the different layers of the dorsal and ventral hippocampus (Figure S2; descriptive statistics in Table S1). Indeed, these analyses show that layers containing astrocytes with less complex backbone structures display higher astrocyte densities (e.g., compare CA1 LacMol and DG Hil with CA1 Rad and DG Mol). Specifically, in the dorsal hippocampus (Figure S2a), CA1 LacMol displays a higher density of astrocytes than CA1 Or ($p = .011$), CA1 Rad ($p < .001$), or DG Mol ($p < .001$). Similarly, DG Hil displays a higher density of astrocytes than CA1 Or ($p = .001$), CA1 Rad ($p < .001$) or DG Mol ($p < .001$). Again, this effect is maintained across the dorsoventral axis, as in the ventral hippocampus (Figure S2b), the CA1 LacMol displays a higher density of astrocytes than CA1 Rad ($p = .040$) and DG Mol ($p = .029$). Similarly, DG Hil displays a higher density of astrocytes than CA1 Or ($p = .022$), CA1 Rad ($p = .004$) or DG Mol ($p = .003$). Furthermore, statistical analyses of cell densities within each hippocampal layer show that astrocyte density is, in fact, maintained along the dorsoventral axis: CA1 Or ($p > .999$); CA1 Rad ($p = .361$); CA1 LacMol ($p = .980$); DG Mol ($p = .822$); DG Hil ($p = .999$).

In summary, these analyses reveal that the heterogeneity of the astrocytic backbone structure observed by more complex astrocytes in the CA1 Rad and DG Mol is highly conserved in the ventral hippocampus. Along the dorsoventral axis, astrocytes in all layers, except in

the DG Mol, display more complex arbors but occupy similar territories, maintaining a constant astrocyte density.

3.3 | Astrocyte exocytosis is crucial for the maintenance of backbone structure

Astrocyte morphology in the adult brain is thought to result (at least in part) from a dynamic interaction with the surrounding environment (Khakh & Sofroniew, 2015; Lanjakornsiripan et al., 2018; Oberheim et al., 2012; Torres-Ceja & Olsen, 2022), with heterogeneity arising due to differences between brain regions. Whereas extrinsic signals might play a role in establishing region (or layer) specific structure difference, little is known about the role of astrocyte signaling in this dynamic interaction. To test whether astrocyte signaling is relevant for the maintenance of backbone structure, GFAP-immunolabeled astrocytes were skeletonized in cryosections containing the dorsal hippocampus of mice lacking exocytosis-dependent signaling in astrocytes (dnSNARE mice) (Pascual et al., 2005), which have been shown to lack SNARE-mediated exocytosis specifically in astrocytes by different laboratories (Halassa et al., 2009; King et al., 2020; Pankratov & Lalo, 2015; Sardinha et al., 2017; Sultan et al., 2015; Zhang et al., 2004). The reconstruction of astrocyte GFAP-immunolabeled structures in cryosections of C57BL/6J mice confirmed that the structural heterogeneity between hippocampal layers described in Figure 1 is maintained under these experimental conditions (Figure S3a–f). First, the astrocytic backbone was reconstructed in the CA1 Rad, where astrocytes display the most complex arbor. This analysis revealed that astrocytes in dnSNARE mice display a simplified morphology (Figure 4a,b). Specifically, astrocytes from CA1 Rad of dnSNARE mice possess shorter process length ($p < .001$, Figure 4c; descriptive statistics in Table S1) and a reduced number of processes ($p < .001$, Figure 4d). This simplified backbone is observed in the Sholl analysis which shows fewer process intersections at 12–24 μm from the soma in dnSNARE mice when compared to WT astrocytes (Figure 4e; statistical details in Table S2). This analysis also shows that, despite the striking structural reduction, the number of main processes (process intersections at 0 μm) and the extension of territory given by the last process intersection radius are maintained (Figure 4f).

To verify whether this reduction in structural complexity was restricted to dnSNARE astrocytes in CA1 Rad, the next step was the reconstruction of astrocytes in the DG Mol. Similarly, astrocytes in the DG Mol of dnSNARE mice display a simplified backbone compared to WT mice (Figure 4g,h). This is translated into a shorter process length ($p < .001$, Figure 4i) and a reduced number of processes ($p < .001$, Figure 4j). Regarding the Sholl analysis, astrocytes from dnSNARE mice display a smaller number of process intersections at 12–20 μm distance from the soma (Figure 4k; statistical details in Table S2). Again, the decreased arbor complexity does not seem to imply a reduction of the total astrocyte territory (Figure 4l). In summary, astrocytic signaling through exocytosis is critical for maintaining the astrocytic backbone in a layer-independent manner, as arbor simplification, in the absence of exocytosis, was observed both in CA1 Rad and DG Mol.

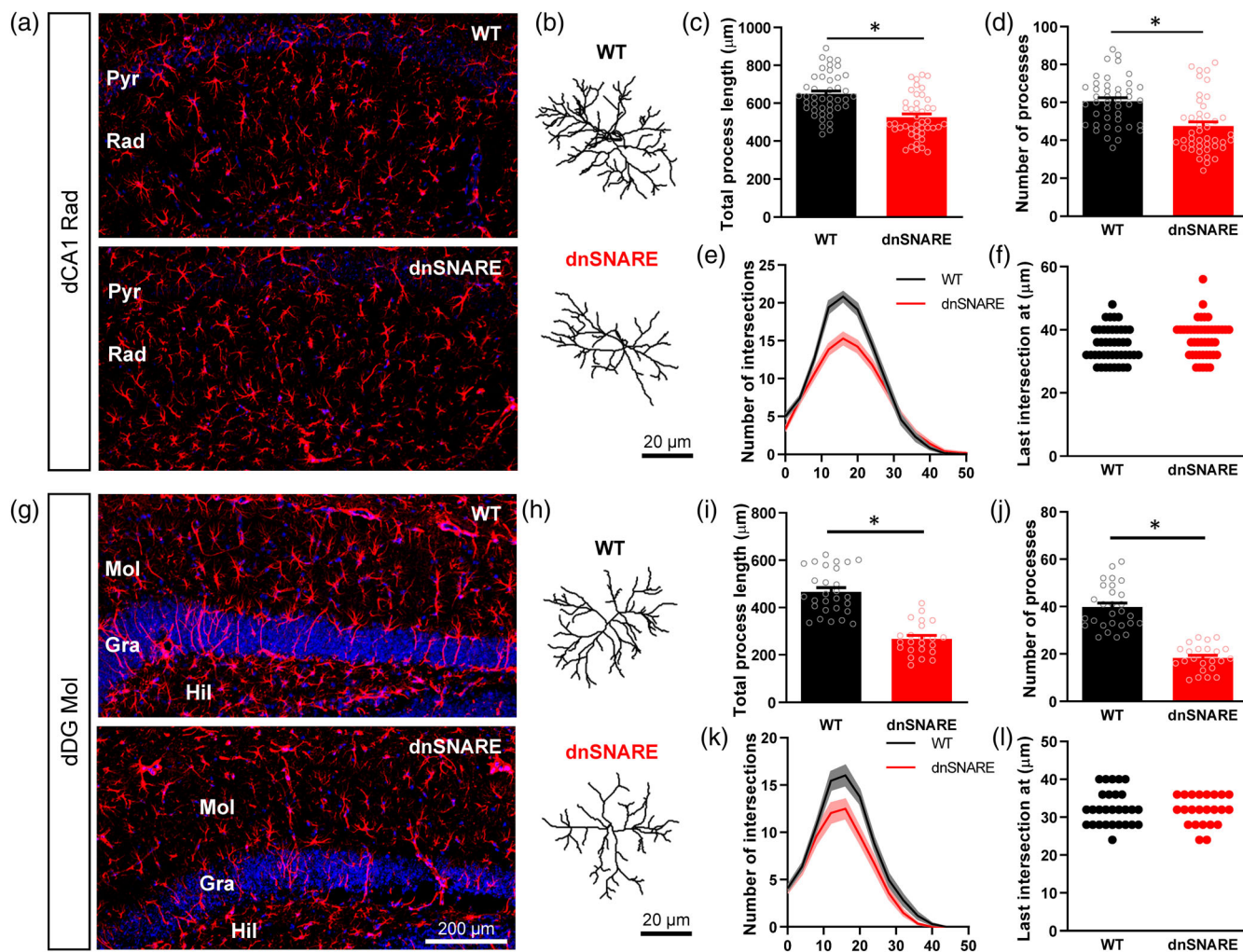


FIGURE 4 Astrocyte exocytosis is required for backbone maintenance. (a) Maximum projection of confocal image z-stacks representing the dorsal CA1 stratum radiatum (dCA1 Rad) of dnSNARE mice immunostained against GFAP (red); (b) representative 3D reconstructions of astrocytes in WT and dnSNARE mice; characterization of 3D astrocytic structures in WT and dnSNARE tissue by analysis of (c) total process length, (d) number of processes, (e) Sholl analysis and (f) last intersection radius; (g) Maximum projection of confocal image z-stacks representative of the dorsal DG stratum moleculare (dDG Mol) of dnSNARE mice stained with anti-GFAP antibody (red). (h) Representative 3D reconstructions of astrocytes in WT and dnSNARE mice. Analysis of morphometric parameters of WT and dnSNARE astrocytes: (i) total process length, (j) number of processes, (k) Sholl analysis, and (l) last intersection radius. Data plotted as individual astrocyte values (dots) and mean \pm SEM (columns and bars). Number of cells: (c–f), WT = 43; dnSNARE = 44 in $N = 5$ mice; Number of cells: (i–l), WT = 28; dnSNARE = 23 in $N = 5$ mice. * $p \leq .05$.

An obvious question, therefore, was whether astrocytic structure could be restored by providing the missing astrocytic signal. To answer this question, sets of WT and dnSNARE mice were i.p. injected with saline or the NMDA-receptor co-agonist D-serine. D-serine appears to be a good candidate to be the putative signaling factor as (i) its extracellular levels can be controlled by astrocytes (Henneberger et al., 2010; Panatier et al., 2006); (ii) inhibition of exocytosis reduces the release of D-serine by astrocytes in different preparations (in vitro, ex vivo and in vivo) (Pankratov & Lalo, 2015; Sultan et al., 2015); and (iii) D-serine supplementation rescued hippocampal function (electrophysiological readouts and cognitive deficits) in dnSNARE mice (Sardinha et al., 2017).

In this new experimental set, brains from WT and dnSNARE mice treated with either saline or D-serine were collected and processed for double immunofluorescent labeling of GFAP and EGFP. Taking advantage of the mosaic-like distribution of EGFP-expressing astrocytes (Fellin et al., 2009; Sardinha et al., 2017), this double labeling allowed us to distinguish anti-GFAP-immunolabeled astrocytes in two groups: EGFP-positive (highly expressing dnSNARE transgenes and thus with reduced exocytosis) and EGFP-negative (reduced expression of dnSNARE transgenes) (Figure 5 left panel). Imaging and skeletonization of the GFAP backbone in CA1 Rad astrocytes in both conditions was compared to WT. Surprisingly, in the CA1 Rad, EGFP-negative astrocytes of dnSNARE mice displayed a similar structure as WT astrocytes, while only EGFP-positive astrocytes displayed the

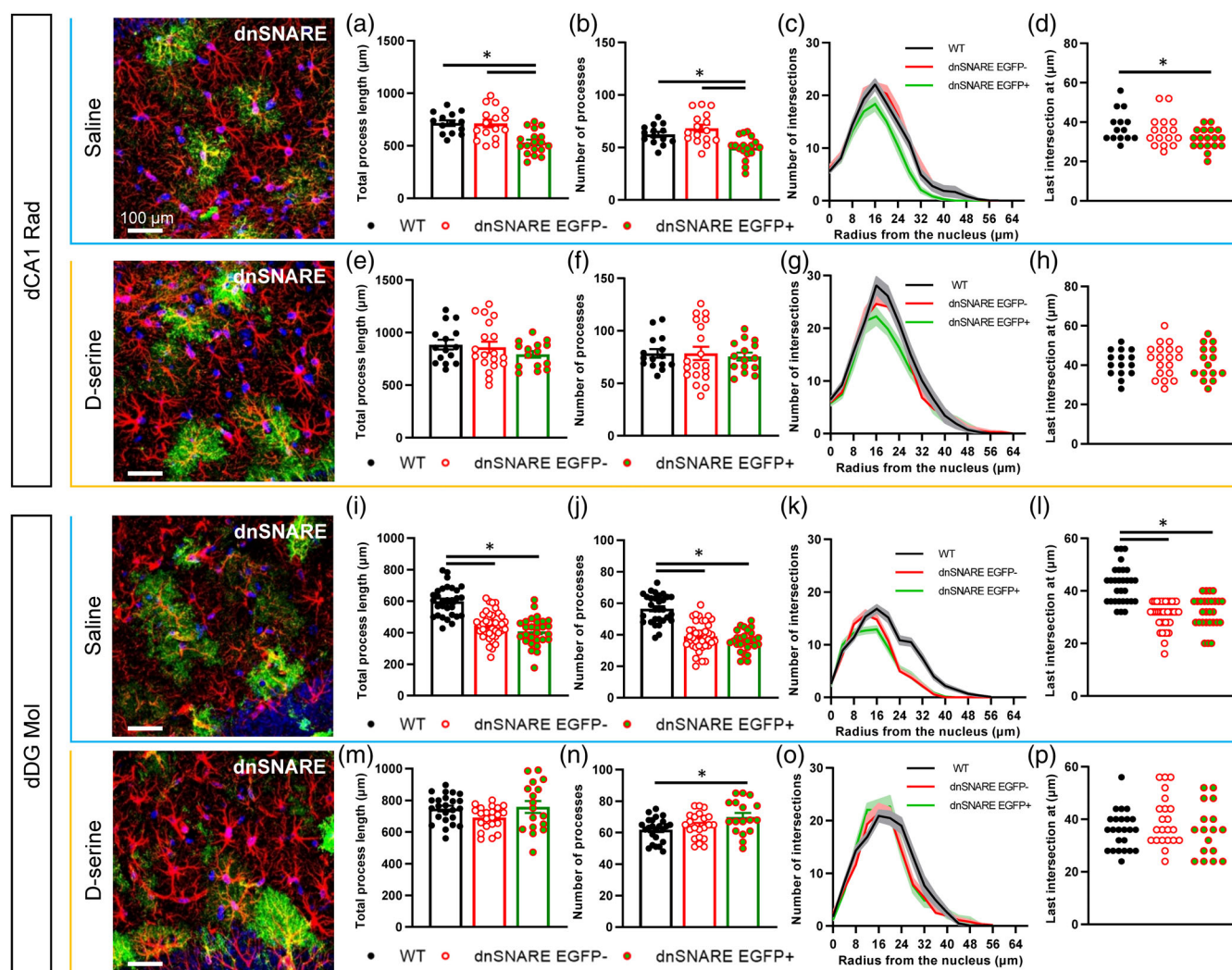


FIGURE 5 Exocytosis-dependent astrocyte signaling sustains backbone structure in a cell-specific manner. (left panel) Maximum projections of confocal image z-stacks representing the CA1 *stratum radiatum* (dCA1 Rad, top) and DG *stratum moleculare* (dDG Mol, bottom) of dnSNARE mice injected with saline or D-serine and subsequently immunolabeled against GFAP (red) and EGFP (green). Characterization of the 3D structures of CA1 *stratum radiatum* astrocytes in WT and dnSNARE mice treated with saline by analysis of (a) total process length, (b) number of processes, (c) Sholl analysis, and (d) last intersection radius. Structural analysis of CA1 *stratum radiatum* astrocytes in WT and dnSNARE injected with D-serine by analysis of (e) total process length, (f) number of processes, (g) Sholl analysis, and (h) last intersection radius. Characterization of the 3D structures of DG *stratum moleculare* astrocytes in WT and dnSNARE mice treated with saline by analysis of (i) total process length, (j) number of processes, (k) Sholl analysis, and (l) last intersection radius. Structural analysis of DG *stratum moleculare* astrocytes in WT and dnSNARE injected with D-serine by analysis of (m) total process length, (n) number of processes, (o) Sholl analysis, and (p) last intersection radius. Data plotted as individual astrocyte values (dots) and mean \pm SEM (columns and bars). Number of cells/group: (a–d) 14, 16, 18; (e–h) 15, 19, 15; (i–l) 30, 39, 28; (m–p) 24, 22, 17 in $N = 2$ WT, 3 dnSNARE mice per condition. $*p \leq .05$.

expected reduction in arbor complexity. This is translated into a decrease in total length ($p < .001$; Figure 5a; descriptive statistics in Table S1) and the number of processes ($p < .010$; Figure 5b). Additionally, dnSNARE EGFP-positive astrocytes were less complex than dnSNARE EGFP-negative and WT astrocytes at 12–32 μm distance from the soma (Figure 5c; statistical details in Table S2). In line with this, dnSNARE EGFP-positive astrocytes display a shorter distance to last process intersection ($p = .041$; Figure 5d). The fact that the backbone of dnSNARE EGFP-negative astrocytes is identical to that of WT astrocytes indicates that the exocytosis-dependent signaling that sustains astrocyte structure in the CA1 Rad, exerts its effects solely

on the affected cell, apparently not propagating to neighboring astrocytes through the extensive astrocyte syncytium (Houades et al., 2006).

Interestingly, D-serine administration rescued the structure of EGFP-positive astrocytes to control levels, making them similar to EGFP-negative astrocytes (Figure 5e–h). This effect was confirmed in terms of total process length (Figure 5e), and the number of processes (Figure 5f). The Sholl analysis indicated that dnSNARE EGFP-positive astrocytes are partially less complex than dnSNARE EGFP-negative and WT astrocytes at 16–24 μm from the soma (Figure 5g; statistical details in Table S2), meaning that the recovery is extensive, but not

complete. Nevertheless, the territory size continues to be similar in the three groups, as given by the Sholl last process intersection (Figure 5h). It is noteworthy that D-serine treatment caused a general increase in astrocyte structure complexity in all groups analyzed in total length ($F_{1,91} = 34.74$; $p < .001$) and number of processes ($F_{1,91} = 25.06$; $p < .001$), and last process intersection ($F_{1,91} = 18.55$; $p < .001$). Further analysis in the dorsal DG Mol of these mice showed that the backbone structure of both EGFP-negative and EGFP-positive astrocytes in dnSNARE mice is less complex in this layer (Figure 5i–l). This is observed in terms of total process length ($p < .001$; Figure 5i), the number of processes ($p < .001$; Figure 5j), Sholl analysis (Figure 5k; statistical details in Table S2), and distance to the last intersection ($p < .001$; Figure 5l). However, Sholl analysis showed that EGFP-positive astrocytes display a partial reduction of structural complexity compared to EGFP-negative astrocytes (Figure 5k; statistical details in Table S2). As in the CA1 Rad, D-serine supplementation rescued the reduction in all parameters analyzed (Figure 5m–p; statistical details in Table S2). Similarly, D-serine treatment caused a general increase in astrocyte structural complexity in the DG Mol, both in terms of total process length ($F_{1,154} = 248.7$; $p < .001$) and the number of processes ($F_{1,154} = 238.5$; $p < .001$).

In summary, cell autonomous, exocytosis-dependent signaling is relevant for maintaining astrocyte backbone structure in different hippocampal subfields. Moreover, this signaling loop appears to involve NMDA receptor co-agonist modulation, as discussed below.

4 | DISCUSSION

For several years, hippocampal astrocytes were considered a homogeneous cell population. However, recent reports describe astrocytes as a heterogeneous population, having distinct transcriptomic profiles that vary between and within brain regions (Batiuk et al., 2020; Bayraktar et al., 2020; Chai et al., 2017; Karpf et al., 2022; Lanjakornsiripan et al., 2018; Morel et al., 2014), suggesting molecular, morphological and functional heterogeneity. The main finding of this work is that hippocampal astrocytes display structural heterogeneity across hippocampal subfields that is conserved along the dorsoventral axis. This finding will be discussed considering the layer-specific nature of the hippocampus, the different levels of morphological complexity, and the existence of a signaling loop that controls astrocytic structure in a cell-specific manner.

4.1 | The layer-specific properties in the hippocampus

Our results show that astrocytes from the CA1 Rad and DG Mol display a more complex backbone when compared to astrocytes from CA1 Or, CA1 LacMol, and DG Hil. Although in line with an earlier report by Ogata and Kosaka (2002), our work provides further structural detail, most noticeably indicating that astrocytes from the CA1 Rad and DG Mol appeared to occupy more extensive areas than hilus

and CA1 LacMol astrocytes. Recently, a report studying structural changes in DG astrocytes during healthy aging suggested that astrocytes from the DG Mol and DG Hil are similar in size and complexity in adulthood (Bondi et al., 2021). The discrepancy with our findings could be explained by the fact that our 3D reconstructions were performed in confocal z-stacks acquired with a 60× magnification revealing GFAP backbones in much greater detail. This is confirmed by much longer process lengths and a higher number of processes reconstructed by our approach (e.g., in the DG Mol). The improvement in detail provided by our preparation and the simplicity of the GFAP staining allowed us to screen backbone complexity in tens of astrocytes in each layer, strengthening the results obtained. Our DG results are also in line with a recent work that described morphologically distinct astrocytes in the DG Mol and DG Hil of the hGFAPeGFP transgenic mouse model (Karpf et al., 2022). We further confirmed these observations in astrocytes from AstroTRAP mice, that were reconstructed based on cytosol-localized GFP signal. It is noteworthy, that despite assessing different details of astrocytic morphology, the inter-layer heterogeneity is still observed. This means that the observed heterogeneity is a robust feature of the hippocampal layers. The complementary analysis of astrocyte densities in the different layers confirms that regions displaying a smaller astrocyte territory, compensate with higher astrocyte densities. These higher densities may be required to maintain the territorial coverage by astrocytes in layers where the astrocytic structure is less complex.

Our data shows that along the dorsoventral axis, astrocytes display more complex arbors (except in the DG Mol). Previous studies showed that the dorsal and ventral hippocampus are structurally similar but functionally, connectively, and transcriptomically different (Beletskiy et al., 2022; Lee et al., 2019; Levone et al., 2021). Moreover, neuro- and astrogliogenesis are differentially regulated in the hippocampal poles (Machado-Santos et al., 2022; Mateus-Pinheiro et al., 2021). Functionally, the dorsal region is linked to cognitive function (e.g., spatial navigation, learning, and memory), while the ventral region is linked to emotional processing (e.g., depressive- and anxious-like behaviors). Our data shows that while the inter-layer heterogeneity in astrocyte structure is maintained along the axis, astrocytes display a more ramified astrocytic structure in a similar volume of ventral layers. Future studies should consider this finding to assess the relevance of more ramified astrocyte structure in integrating neuroglial circuits (of existing and newborn astrocytes) connected to brain regions involved in emotion-processing.

Further studies using automatic approaches to assess a larger number of cells, such as the approach used by Refaeli et al. (2021), should provide additional details on astrocyte structure across the hippocampal layers: to date, Refaeli and colleagues have also reported on the structure of CA1 Rad astrocytes and their approximate densities in the brain tissue, data which largely aligns with our findings.

Furthermore, our finding of astrocytic structural heterogeneity across the hippocampus is in line with a recent elegant study showing that neocortical astrocytes have distinct morphologies across the cortical layers (Lanjakornsiripan et al., 2018). This study suggests that the mature astrocytic structure depends on the neuronal organization of



each cortical layer, structural interactions with synapses, and molecular expression profiles. In the cortex, astrocyte morphogenesis was shown to depend on direct contact with neuronal processes and to occur in parallel with the growth and activity of synaptic circuits (Stogsdill et al., 2017). Another possibility is the regulation of astrocyte structure by excitatory signaling that follows the layer-specific distribution of glutamatergic neurons (Morel et al., 2014). As in the cortex, the hippocampus is also organized in different layers with specific organization of neuronal populations (Andersen et al., 2007). On the one hand, astrocytes in the CA1 Rad and DG Mol are surrounded by bundles of axons establishing excitatory synapses upon pyramidal and granule cell dendrites, respectively. This excitatory environment could dictate the large size of the astrocyte territory in comparison, for instance, with hilar astrocytes. On the other hand, astrocytes in the CA1 Or and the CA1 LacMol are also surrounded by axons establishing excitatory synapses with basal and distal apical dendrites of pyramidal neurons. Still, their backbone size is relatively less complex. Interestingly, a recent study showed that astrocyte GluN2C NMDA receptors tune synaptic strengths in CA1 pyramidal neurons in a layer-specific manner. While this effect requires CA1 Rad astrocytes, interfering with astrocytic NMDARs has little effect on synaptic strength diversity in the CA1 Or or CA1 LacMol (Chipman et al., 2021). Further studies should address a link between synaptic strength and astrocyte morphology in a layer-specific manner.

Although there is still no obvious explanation for the structural heterogeneity across layers and the increased structural complexity along the dorsoventral axis, further studies should consider different aspects such as the origin of afferent axons, synaptic activity levels, the density of excitatory versus inhibitory synapses, and the availability of space (considering evolutionary spatial constraints). Indeed, recent transcriptional studies from our laboratory and others proposed different astrocytic morphological properties based on local molecular expression (Batiuk et al., 2020; Endo et al., 2022), suggesting that astrocytic structure might result from concerted neuroglial signaling following the cytoarchitecture of a particular layer. This type of local signaling may also explain why astrocyte clones scattered through the cortex can adopt unique morphologies (Clavreul et al., 2019; Lanjakornsiripan et al., 2018).

4.2 | The different levels of morphological complexity

Our anti-GFAP staining and AstroTRAP results confirm the heterogeneity of the astrocytic backbone, which represents the first “macroscopic” level of morphology. However, the volume fraction analysis, that provides quantification of the second level of morphology, namely finer structures (e.g., leaflets) (Minge et al., 2021), did not overlap completely with the backbone results, especially in the DG Hil. Together, these findings suggest that morphological heterogeneity occurs independently on different morphological levels (backbone vs. leaflets), across the five regions. For instance, CA1 Rad and DG Mol astrocytes have the most GFAP-positive and AstroTRAP-positive

main processes and the largest overall territories but fill this volume with an average amount of processes (given by volume fraction). In comparison, DG Hil astrocytes have a less elaborate GFAP-defined backbone and a smaller overall territory, but volume fraction analysis reveals that they, in total, occupy a higher percentage of volume in their territories. Finally, astrocytes in the CA1 LacMol and CA1 Or have a simpler backbone and occupy a lower percentage of tissue volume within their territories. This suggests that the two levels of astrocyte morphology might be regulated independently between layers.

4.3 | The existence of a signaling loop that controls astrocytic structure

While our data are in line with a layer-specific heterogeneity of the astrocyte backbone structure that might be regulated by extrinsic signals (discussed earlier), they also suggest that astrocyte exocytosis is part of a signaling loop involved in the regulation of the backbone structure in a cell-specific manner. Exocytosis-dependent signaling is critical for the maintenance of the astrocyte backbone across different hippocampal layers, as its inhibition leads to a reduction in backbone complexity of ~25%. Moreover, in the CA1 Rad this is a local cell-specific mechanism as the structure of neighboring EGFP-negative astrocytes is unaffected. One should consider that an imbalance of exocytosis versus endocytosis could affect membrane turnover that could lead to, at least partially, a reduction in structural complexity. However, this does not seem to be the case because the number of vesicles available for exocytosis appear too low (Aten et al., 2022) to cause the dramatic trafficking imbalance necessary to produce such structural consequence. Moreover, D-serine supplementation rescued astrocyte backbone complexity, even in astrocytes in which exocytosis was impaired (EGFP-positive). This favors a signaling-dependent mechanism of regulation rather than an imbalance in membrane turnover.

D-serine administration restored astrocyte structure in the CA1 Rad and DG Mol to similar levels, supporting a general signaling mechanism across the hippocampal layers. Although D-serine rescued the astrocytic backbone structure, our experiments do not prove that D-serine is the molecule released from astrocytic vesicles. To our knowledge, the only direct biological target of D-serine in the mammalian body is the NMDA receptor co-agonist binding site, which has two endogenous ligands: D-serine and glycine. Therefore, our experiments suggest an involvement of the co-agonist binding site. An effect of i.p.-injected D-serine via the co-agonist binding site is also consistent with the findings by Robin et al. (2018) that i.p.-injected compounds, such as MK-801 and D-serine, modify NMDAR-dependent hippocampal LTP and object recognition memory, respectively. Such experiments on their own do not rule out the involvement of other co-agonists like glycine, as saturation of NMDA receptors with exogenous D-serine could compensate reduced glycine levels. However, we are not aware of experimental evidence indicating astrocytic control of extracellular glycine levels by vesicular release. It is therefore most likely that the effects are due to reduced D-serine levels. While there is still a debate about the relative contribution of

astrocytes and neurons in regulating extracellular D-serine levels (Papouin, Henneberger, et al., 2017; Wolosker et al., 2016), it is indisputable that D-serine is a crucial modulator of synaptic transmission and plasticity and that its availability is regulated by astrocytes (Adamsky et al., 2018; Bohmbach et al., 2022; Fossat et al., 2012; Henneberger et al., 2010, 2020; Papouin, Dunphy, et al., 2017; Robin et al., 2018; Takata et al., 2011; Yang et al., 2003). Nonetheless, the magnitude of the D-serine effect could differ between brain regions, because the balance between D-serine and glycine as co-agonists of the NMDA receptor depends on the brain region (Bail et al., 2015). This might explain the lack of striking differences in astrocytic structure between EGFP-positive and EGFP-negative astrocytes in the DG Mol compared to the CA1 Rad. Our data showing that D-serine supplementation rescues astrocyte complexity, in the absence of astrocytic exocytosis, might help to understand the electrophysiologic restoration of hippocampus-prefrontal cortex synchrony observed in our previous study (Sardinha et al., 2017). Moreover, this functional rescue might have also contributed to the observed cognitive recovery of dnSNARE mice treated with D-serine (Sardinha et al., 2017). D-Serine acts on NMDARs, which are primarily neuronal, to support neuronal power and long-distance neuronal synchronization (Sardinha et al., 2017), synaptic transmission (Adamsky et al., 2018; Henneberger et al., 2010, 2020) and dendritic spike integration (Bohmbach et al., 2022). Our data suggest a signaling loop in which astrocytic D-serine and neuronal glutamate release jointly modulate astrocyte morphology. Indeed, there is evidence supporting such a mechanism, at least in the developing cortex, where glutamatergic signaling was shown to be involved in the determination of the morphological properties of astrocytes (Morel et al., 2014; Zehnder et al., 2021). Moreover, the observation that D-serine also causes a general increase in astrocyte structure complexity across the different hippocampal layers is in line with our previous electrophysiological observation of a general increase in neuronal power activity observed in all frequency bands in the hippocampus (Sardinha et al., 2017). While we believe this is the most parsimonious explanation for D-serine action, we cannot exclude, however, that expression of the dnSNARE itself could affect the levels of GFAP expression in cells. Future studies should address this issue specifically.

In summary, astrocytes appear to contribute with an exocytosis-dependent signaling loop to the self-maintenance of backbone structure. This signaling loop does not seem responsible for determining the aforementioned inter-layer backbone heterogeneity, where surrounding neuro-glial cues may play a more relevant role.

The main finding of this study is that astrocytes display backbone heterogeneity across the hippocampal layers, which is conserved along the dorsoventral axis. There are, however, several open questions that need to be addressed. What are the layer-specific signals that dictate astrocytic backbone structure? Is there a requirement for a more complex backbone structure for circuits related to emotional processing in the ventral hippocampus? Which is the net relation between the backbone structure, leaflet distribution, and synaptic coverage? Which are the signals involved in the signaling loop that supports astrocyte backbone structure?

The current development of techniques that allow more efficient cell structure labeling and imaging and the advent of spatial sequencing will hopefully provide us with information on astrocyte morphological complexity and plasticity to answer these questions.

AUTHOR CONTRIBUTIONS

JFV, JLM, and JFO designed the project, supervised the data analysis, and wrote the manuscript. JFV, JLM, DSA, AV, SB, GT, MM, VMS, SGG, CD, AP, JW, CL performed the experiments and analyzed the results. CC, CH, MGH, and JFO contributed with intellectual content and critical manuscript review.

ACKNOWLEDGMENTS

The authors acknowledge the Foundation for Science and Technology (FCT) fellowships to João Filipe Viana, João Luís Machado, and Daniela Sofia Abreu. IF grant to João Filipe Pedreira de Oliveira (IF/00328/2015); projects PTDC/MED-NEU/31417/2017 and POCI-01-0145-FEDER-016818; grants from Bial Foundation (037/18) and “la Caixa” Foundation (LCF/PR/HR21/52410024) to João Filipe Pedreira de Oliveira; ICVS Scientific Microscopy Platform, member of the national infrastructure PPBI—Portuguese Platform of Bioimaging (PPBI-POCI-01-0145-FEDER-022122); by National funds, through the Foundation for Science and Technology (FCT)—project UIDB/50026/2020 and UIDP/50026/2020. Cátia Domingos was enrolled in the International Max Planck Research School (IMPRS) for Brain and Behavior (Bonn, Germany). Experiments in CH's laboratory were supported by the German Research Foundation (DFG; SFB1089 B03, SPP1757 HE6949/1 and HE6949/3) and the European Union (EU, H2020-MSCA-ITN project 722053 EU-GliaPhD). Matthew G. Holt was supported by Fonds Wetenschappelijk Onderzoek (FWO) Grant G066715N, KU Leuven Internal Funding (C1 grant) (C14/20/071) and European Research Council (ERC) Grant 281961 (AstroFunc). He currently holds the ERA Chair (NCBio) at i3S Porto, funded by the European Commission (H2020-WIDESPREAD-2018-2020-6; NCBio; 951923). Jérôme Wahis acknowledges the receipt of FWO post-doctoral fellowships (12V7519N and 12V7522N) and research grant (1513020N).

DATA AVAILABILITY STATEMENT

The data that supports the findings of this study are available in the supplementary material of this article (Table S1). Detailed datasets may be made available from the corresponding author upon request.

ORCID

Corrado Cali  <https://orcid.org/0000-0003-4856-0835>

Christian Henneberger  <https://orcid.org/0000-0002-5391-7387>

Matthew G. Holt  <https://orcid.org/0000-0002-8958-4027>

João Filipe Oliveira  <https://orcid.org/0000-0002-1005-2328>

REFERENCES

- Adamsky, A., Kol, A., Kreisel, T., Doron, A., Ozeri-Engelhard, N., Melcer, T., Refaeli, R., Horn, H., Regev, L., Groysman, M., London, M., & Goshen, I. (2018). Astrocytic activation generates de novo neuronal potentiation



- and memory enhancement. *Cell*, 174(1), 59–71.e14. <https://doi.org/10.1016/j.cell.2018.05.002>
- Anders, S., Minge, D., Griemsmann, S., Herde, M. K., Steinhäuser, C., & Henneberger, C. (2014). Spatial properties of astrocyte gap junction coupling in the rat hippocampus. *Philosophical Transactions of the Royal Society B: Biological Sciences*, 369(1654), 20130600. <https://doi.org/10.1098/rstb.2013.0600>
- Andersen, P., Morris, R., Amaral, D., O'Keefe, J., & Bliss, T. (2007). *The hippocampus book*. Oxford University Press.
- Araque, A., Carmignoto, G., Haydon, P. G., Oliet, S. H. R., Robitaille, R., & Volterra, A. (2014). Gliotransmitters travel in time and space. *Neuron*, 81(4), 728–739. <https://doi.org/10.1016/j.neuron.2014.02.007>
- Arizono, M., Inavalli, V. V. G. K., Bancelin, S., Fernández-Monreal, M., & Nägerl, U. V. (2021). Super-resolution shadow imaging reveals local remodeling of astrocytic microstructures and brain extracellular space after osmotic challenge. *Glia*, 69(6), 1605–1613. <https://doi.org/10.1002/glia.23995>
- Arizono, M., & Nägerl, U. V. (2022). Deciphering the functional nano-anatomy of the tripartite synapse using stimulated emission depletion microscopy. *Glia*, 70(4), 607–618. <https://doi.org/10.1002/glia.24103>
- Aten, S., Kiyoshi, C. M., Arzola, E. P., Patterson, J. A., Taylor, A. T., Du, Y., Guiher, A. M., Philip, M., Camacho, E. G., Mediratta, D., Collins, K., Boni, K., Garcia, S. A., Kumar, R., Drake, A. N., Hegazi, A., Trank, L., Benson, E., Kidd, G., ... Zhou, M. (2022). Ultrastructural view of astrocyte arborization, astrocyte-astrocyte and astrocyte-synapse contacts, intracellular vesicle-like structures, and mitochondrial network. *Progress in Neurobiology*, 213, 102264. <https://doi.org/10.1016/j.pneurobio.2022.102264>
- Bail, M. L., Martineau, M., Sacchi, S., Yatsenko, N., Radziszewsky, I., Conrod, S., Ouares, K. A., Wolosker, H., Pollegioni, L., Billard, J.-M., & Mothet, J.-P. (2015). Identity of the NMDA receptor coagonist is synapse specific and developmentally regulated in the hippocampus. *Proceedings of the National Academy of Sciences of the United States of America*, 112(2), E204–E213. <https://doi.org/10.1073/pnas.1416668112>
- Batiuk, M. Y., Martirosyan, A., Wahis, J., de Vin, F., Marneffe, C., Kusserow, C., Koeppen, J., Viana, J. F., Oliveira, J. F., Voet, T., Ponting, C. P., Belgard, T. G., & Holt, M. G. (2020). Identification of region-specific astrocyte subtypes at single cell resolution. *Nature Communications*, 11(1), Article 1. <https://doi.org/10.1038/s41467-019-14198-8>
- Bayraktar, O. A., Bartels, T., Holmqvist, S., Kleshchevnikov, V., Martirosyan, A., Polioudakis, D., Haim, L. B., Young, A. M. H., Batiuk, M. Y., Prakash, K., Brown, A., Roberts, K., Paredes, M. F., Kawaguchi, R., Stockley, J. H., Sabeur, K., Chang, S. M., Huang, E., Hutchinson, P., ... Rowitch, D. H. (2020). Astrocyte layers in the mammalian cerebral cortex revealed by a single-cell in situ transcriptomic map. *Nature Neuroscience*, 1–10, 500–509. <https://doi.org/10.1038/s41593-020-0602-1>
- Beletskiy, A., Positselskaya, E., Vinarskaya, A. K., Spivak, Y. S., Dobryakova, Y. V., Tyulenev, I., Markevich, V. A., & Bolshakov, A. P. (2022). Detailed analysis of dorsal-ventral gradients of gene expression in the hippocampus of adult rats. *International Journal of Molecular Sciences*, 23(17), Article 17. <https://doi.org/10.3390/ijms23179948>
- Bernardinelli, Y., Randall, J., Janett, E., Nikonenko, I., König, S., Jones, E. V., Flores, C. E., Murai, K. K., Bochet, C. G., Holtmaat, A., & Müller, D. (2014). Activity-dependent structural plasticity of perisynaptic astrocytic domains promotes excitatory synapse stability. *Current Biology*, 24(15), 1679–1688. <https://doi.org/10.1016/j.cub.2014.06.025>
- Bohmbach, K., Masala, N., Schönhense, E. M., Hill, K., Haubrich, A. N., Zimmer, A., Oplitz, T., Beck, H., & Henneberger, C. (2022). An astrocytic signaling loop for frequency-dependent control of dendritic integration and spatial learning. *Nature Communications*, 13(1), Article 1. <https://doi.org/10.1038/s41467-022-35620-8>
- Bondi, H., Bortolotto, V., Canonico, P. L., & Grilli, M. (2021). Complex and regional-specific changes in the morphological complexity of GFAP+ astrocytes in middle-aged mice. *Neurobiology of Aging*, 100, 59–71. <https://doi.org/10.1016/j.neurobiolaging.2020.12.018>
- Bushong, E. A., Martone, M. E., Jones, Y. Z., & Ellisman, M. H. (2002). Protoplasmic astrocytes in CA1 stratum radiatum occupy separate anatomical domains. *The Journal of Neuroscience*, 22(1), 183–192.
- Calì, C., Agus, M., Kare, K., Boges, D. J., Lehväläiho, H., Hadwiger, M., & Magistretti, P. J. (2019). 3D cellular reconstruction of cortical glia and parenchymal morphometric analysis from serial block-face electron microscopy of juvenile rat. *Progress in Neurobiology*, 183, 101696. <https://doi.org/10.1016/j.pneurobio.2019.101696>
- Chai, H., Diaz-Castro, B., Shigetomi, E., Monte, E., Oceau, J. C., Yu, X., Cohn, W., Rajendran, P. S., Vondriska, T. M., Whitelegge, J. P., Coppola, G., & Khakh, B. S. (2017). Neural circuit-specialized astrocytes: Transcriptomic, proteomic, morphological, and functional evidence. *Neuron*, 95(3), 531–549.e9. <https://doi.org/10.1016/j.neuron.2017.06.029>
- Chipman, P. H., Fung, C. C. A., Pazo Fernandez, A., Sawant, A., Tedoldi, A., Kawai, A., Ghimire Gautam, S., Kurosawa, M., Abe, M., Sakimura, K., Fukai, T., & Goda, Y. (2021). Astrocyte GluN2C NMDA receptors control basal synaptic strengths of hippocampal CA1 pyramidal neurons in the stratum radiatum. *eLife*, 10, e70818. <https://doi.org/10.7554/eLife.70818>
- Clavreul, S., Abdeladim, L., Hernández-Garzón, E., Niculescu, D., Durand, J., Ieng, S.-H., Barry, R., Bonvento, G., Beaurepaire, E., Livet, J., & Loulier, K. (2019). Cortical astrocytes develop in a plastic manner at both clonal and cellular levels. *Nature Communications*, 10(1), 1–14. <https://doi.org/10.1038/s41467-019-12791-5>
- de Oliveira Figueiredo, E. C., Calì, C., Petrelli, F., & Bezzi, P. (2022). Emerging evidence for astrocyte dysfunction in schizophrenia. *Glia*, 70(9), 1585–1604. <https://doi.org/10.1002/glia.24221>
- Eilam, R., Aharoni, R., Arnon, R., & Malach, R. (2016). Astrocyte morphology is confined by cortical functional boundaries in mammals ranging from mice to human. *eLife*, 5, e15915. <https://doi.org/10.7554/eLife.15915>
- Emsley, J. G., & Macklis, J. D. (2006). Astroglial heterogeneity closely reflects the neuronal-defined anatomy of the adult murine CNS. *Neuron Glia Biology*, 2(3), 175–186. <https://doi.org/10.1017/S1740925X06000202>
- Endo, F., Kasai, A., Soto, J. S., Yu, X., Qu, Z., Hashimoto, H., Gradinaru, V., Kawaguchi, R., & Khakh, B. S. (2022). Molecular basis of astrocyte diversity and morphology across the CNS in health and disease. *Science*, 378(6619), eadc9020. <https://doi.org/10.1126/science.adc9020>
- Fellin, T., Halassa, M. M., Terunuma, M., Succol, F., Takano, H., Frank, M., Moss, S. J., & Haydon, P. G. (2009). Endogenous nonneuronal modulators of synaptic transmission control cortical slow oscillations in vivo. *Proceedings of the National Academy of Sciences of the United States of America*, 106(35), 15037–15042.
- Fossat, P., Turpin, F. R., Sacchi, S., Dulong, J., Shi, T., Rivet, J.-M., Sweedler, J. V., Pollegioni, L., Millan, M. J., Oliet, S. H. R., & Mothet, J.-P. (2012). Glial D-serine gates NMDA receptors at excitatory synapses in prefrontal cortex. *Cerebral Cortex*, 22(3), 595–606. <https://doi.org/10.1093/cercor/bhr130>
- Genoud, C., Quairiaux, C., Steiner, P., Hirling, H., Welker, E., & Knott, G. W. (2006). Plasticity of astrocytic coverage and glutamate transporter expression in adult mouse cortex. *PLoS Biology*, 4(11), e343. <https://doi.org/10.1371/journal.pbio.0040343>
- Grosche, A., Grosche, J., Tackenberg, M., Scheller, D., Gerstner, G., Gumprecht, A., Pannicke, T., Hirrlinger, P. G., Wilhelmsson, U., Hüttmann, K., Härtig, W., Steinhäuser, C., Pekny, M., & Reichenbach, A. (2013). Versatile and simple approach to determine astrocyte territories in mouse neocortex and hippocampus. *PLoS One*, 8(7), e69143. <https://doi.org/10.1371/journal.pone.0069143>
- Guercio, G. D., Bevilacqua, L., Vargas-Lopes, C., Madeira, C., Oliveira, A., Carvalho, V. F., d'Avila, J. C., & Panizzutti, R. (2014). D-serine prevents

- cognitive deficits induced by acute stress. *Neuropharmacology*, 86, 1–8. <https://doi.org/10.1016/j.neuropharm.2014.06.021>
- Halassa, M. M., Florian, C., Fellin, T., Munoz, J. R., Lee, S.-Y., Abel, T., Haydon, P. G., & Frank, M. G. (2009). Astrocytic modulation of sleep homeostasis and cognitive consequences of sleep loss. *Neuron*, 61(2), 213–219. <https://doi.org/10.1016/j.neuron.2008.11.024>
- Han, H., Peng, Y., & Dong, Z. (2015). D-serine rescues the deficits of hippocampal long-term potentiation and learning and memory induced by sodium fluoroacetate. *Pharmacology Biochemistry and Behavior*, 133, 51–56. <https://doi.org/10.1016/j.pbb.2015.03.017>
- Henneberger, C., Bard, L., Panatier, A., Reynolds, J. P., Kopach, O., Medvedev, N. I., Minge, D., Herde, M. K., Anders, S., Kraev, I., Heller, J. P., Rama, S., Zheng, K., Jensen, T. P., Sanchez-Romero, I., Jackson, C. J., Janovjak, H., Ottersen, O. P., Nagelhus, E. A., ... Rusakov, D. A. (2020). LTP induction boosts glutamate spillover by driving withdrawal of perisynaptic astroglia. *Neuron*, 108(5), 919–936. <https://doi.org/10.1016/j.neuron.2020.08.030>
- Henneberger, C., Papouin, T., Oliet, S. H. R., & Rusakov, D. A. (2010). Long-term potentiation depends on release of D-serine from astrocytes. *Nature*, 463(7278), 232–236. <https://doi.org/10.1038/nature08673>
- Herde, M. K., Bohmbach, K., Domingos, C., Vana, N., Komorowska-Müller, J. A., Passlick, S., Schwarz, I., Jackson, C. J., Dietrich, D., Schwarz, M. K., & Henneberger, C. (2020). Local efficacy of glutamate uptake decreases with synapse size. *Cell Reports*, 32(12), 108182. <https://doi.org/10.1016/j.celrep.2020.108182>
- Hirrlinger, J., & Nimmerjahn, A. (2022). A perspective on astrocyte regulation of neural circuit function and animal behavior. *Glia*, 70, 1554–1580. <https://doi.org/10.1002/glia.24168>
- Houades, V., Rouach, N., Ezan, P., Kirchhoff, F., Koulakoff, A., & Giaume, C. (2006). Shapes of astrocyte networks in the juvenile brain. *Neuron Glia Biology*, 2(1), 3–14. <https://doi.org/10.1017/S1740925X06000081>
- Jones, M. E., Paniccia, J. E., Lebonville, C. L., Reissner, K. J., & Lysle, D. T. (2018). Chemogenetic manipulation of dorsal hippocampal astrocytes protects against the development of stress-enhanced fear learning. *Neuroscience*, 388, 45–56. <https://doi.org/10.1016/j.neuroscience.2018.07.015>
- Karpf, J., Unichenko, P., Chalmers, N., Beyer, F., Wittmann, M.-T., Schneider, J., Fidan, E., Reis, A., Beckervordersandforth, J., Brandner, S., Liebner, S., Falk, S., Sagner, A., Henneberger, C., & Beckervordersandforth, R. (2022). Dentate gyrus astrocytes exhibit layer-specific molecular, morphological and physiological features. *Nature Neuroscience*, 25(12), Article 12–Article 1638. <https://doi.org/10.1038/s41593-022-01192-5>
- Khakh, B. S., & Sofroniew, M. V. (2015). Diversity of astrocyte functions and phenotypes in neural circuits. *Nature Neuroscience*, 18(7), 942–952. <https://doi.org/10.1038/nn.4043>
- King, A. C., Wood, T. E., Rodríguez, E., Parpura, V., & Gray, M. (2020). Differential effects of SNARE-dependent gliotransmission on behavioral phenotypes in a mouse model of Huntington's disease. *Experimental Neurology*, 330, 113358. <https://doi.org/10.1016/j.expneurol.2020.113358>
- Lanjakornsiripan, D., Pior, B.-J., Kawaguchi, D., Furutachi, S., Tahara, T., Katsuyama, Y., Suzuki, Y., Fukazawa, Y., & Gotoh, Y. (2018). Layer-specific morphological and molecular differences in neocortical astrocytes and their dependence on neuronal layers. *Nature Communications*, 9(1), Article 1. <https://doi.org/10.1038/s41467-018-03940-3>
- Lavialle, M., Aumann, G., Anlauf, E., Pröls, F., Arpin, M., & Derouiche, A. (2011). Structural plasticity of perisynaptic astrocyte processes involves ezrin and metabotropic glutamate receptors. *Proceedings of the National Academy of Sciences of the United States of America*, 108(31), 12915–12919. <https://doi.org/10.1073/pnas.1100957108>
- Lee, S. L. T., Lew, D., Wickenheisser, V., & Markus, E. J. (2019). Interdependence between dorsal and ventral hippocampus during spatial navigation. *Brain and Behavior*, 9(10), e01410. <https://doi.org/10.1002/brb3.1410>
- Levone, B. R., Moloney, G. M., Cryan, J. F., & O'Leary, O. F. (2021). Specific sub-regions along the longitudinal axis of the hippocampus mediate antidepressant-like behavioral effects. *Neurobiology of Stress*, 14, 100331. <https://doi.org/10.1016/j.ynstr.2021.100331>
- Livet, J., Weissman, T. A., Kang, H., Draft, R. W., Lu, J., Bennis, R. A., Sanes, J. R., & Lichtman, J. W. (2007). Transgenic strategies for combinatorial expression of fluorescent proteins in the nervous system. *Nature*, 450(7166), 56–62. <https://doi.org/10.1038/nature06293>
- Lushnikova, I., Skibo, G., Muller, D., & Nikonenko, I. (2009). Synaptic potentiation induces increased glial coverage of excitatory synapses in CA1 hippocampus. *Hippocampus*, 19(8), 753–762. <https://doi.org/10.1002/hipo.20551>
- Machado-Santos, A. R., Loureiro-Campos, E., Patrício, P., Araújo, B., Alves, N. D., Mateus-Pinheiro, A., Correia, J. S., Morais, M., Bessa, J. M., Sousa, N., Rodrigues, A. J., Oliveira, J. F., & Pinto, L. (2022). Beyond new neurons in the adult hippocampus: Imipramine acts as a pro-astroglial factor and rescues cognitive impairments induced by stress exposure. *Cell*, 11(3), Article 3. <https://doi.org/10.3390/cells11030390>
- Mateus-Pinheiro, A., Patrício, P., Alves, N. D., Martins-Macedo, J., Caetano, I., Silveira-Rosa, T., Araújo, B., Mateus-Pinheiro, M., Silva-Correia, J., Sardinha, V. M., Loureiro-Campos, E., Rodrigues, A. J., Oliveira, J. F., Bessa, J. M., Sousa, N., & Pinto, L. (2021). Hippocampal cytotogenesis abrogation impairs inter-regional communication between the hippocampus and prefrontal cortex and promotes the time-dependent manifestation of emotional and cognitive deficits. *Molecular Psychiatry*, 1–13, 7154–7166. <https://doi.org/10.1038/s41380-021-01287-8>
- Minge, D., Domingos, C., Unichenko, P., Behringer, C., Pauletti, A., Anders, S., Herde, M. K., Delekate, A., Gulakova, P., Schoch, S., Petzold, G. C., & Henneberger, C. (2021). Heterogeneity and development of fine astrocyte morphology captured by diffraction-limited microscopy. *Frontiers in Cellular Neuroscience*, 15. <https://doi.org/10.3389/fncel.2021.669280>
- Morel, L., Higashimori, H., Tolman, M., & Yang, Y. (2014). VGluT1+ neuronal glutamatergic signaling regulates postnatal developmental maturation of cortical protoplasmic astroglia. *Journal of Neuroscience*, 34(33), 10950–10962. <https://doi.org/10.1523/JNEUROSCI.1167-14.2014>
- Nagai, J., Yu, X., Papouin, T., Cheong, E., Freeman, M. R., Monk, K. R., Hastings, M. H., Haydon, P. G., Rowitch, D., Shaham, S., & Khakh, B. S. (2020). Behaviorally consequential astrocytic regulation of neural circuits. *Neuron*, 109(4), 576–596. <https://doi.org/10.1016/j.neuron.2020.12.008>
- Navarrete, M., Cuartero, M. I., Palenzuela, R., Draffin, J. E., Konomi, A., Serra, I., Colié, S., Castaño-Castaño, S., Hasan, M. T., Nebreda, Á. R., & Esteban, J. A. (2019). Astrocytic p38 α MAPK drives NMDA receptor-dependent long-term depression and modulates long-term memory. *Nature Communications*, 10(1), 2968. <https://doi.org/10.1038/s41467-019-10830-9>
- Nolte, C., Matyash, M., Pivneva, T., Schipke, C.-G., Ohlemeyer, C., Hanisch, U. K., Kirchhoff, F., & Kettenmann, H. (2001). GFAP promoter-controlled EGFP-expressing transgenic mice: A tool to visualize astrocytes and astrogliosis in living brain tissue. *Glia*, 33(1), 72–86.
- Oberheim, N. A., Goldman, S. A., & Nedergaard, M. (2012). Heterogeneity of astrocytic form and function. *Methods in Molecular Biology*, 814, 23–45. https://doi.org/10.1007/978-1-61779-452-0_3
- Oberheim, N. A., Takano, T., Han, X., He, W., Lin, J. H. C., Wang, F., Xu, Q., Wyatt, J. D., Pilcher, W., Ojemann, J. G., Ransom, B. R., Goldman, S. A., & Nedergaard, M. (2009). Uniquely hominid features of adult human astrocytes. *The Journal of Neuroscience*, 29(10), 3276–3287. <https://doi.org/10.1523/JNEUROSCI.4707-08.2009>
- Ogata, K., & Kosaka, T. (2002). Structural and quantitative analysis of astrocytes in the mouse hippocampus. *Neuroscience*, 113(1), 221–233. [https://doi.org/10.1016/S0306-4522\(02\)00041-6](https://doi.org/10.1016/S0306-4522(02)00041-6)
- Oliveira, J. F., & Araque, A. (2022). Astrocyte regulation of neural circuit activity and network states. *Glia*, 70, 1455–1466. <https://doi.org/10.1002/glia.24178>
- Oliveira, J. F., Sardinha, V. M., Guerra-Gomes, S., Araque, A., & Sousa, N. (2015). Do stars govern our actions? Astrocyte involvement in rodent behavior. *Trends in Neurosciences*, 38(9), 535–549. <https://doi.org/10.1016/j.tins.2015.07.006>



- Panatier, A., Theodosis, D. T., Mothet, J.-P., Touquet, B., Pollegioni, L., Poulain, D. A., & Oliet, S. H. R. (2006). Glia-derived d-serine controls NMDA receptor activity and synaptic memory. *Cell*, 125(4), 775–784. <https://doi.org/10.1016/j.cell.2006.02.051>
- Pankratov, Y., & Lalo, U. (2015). Role for astroglial α 1-adrenoreceptors in gliotransmission and control of synaptic plasticity in the neocortex. *Frontiers in Cellular Neuroscience*, 9. <https://doi.org/10.3389/fncel.2015.00230>
- Papouin, T., Dunphy, J. M., Tolman, M., Dineley, K. T., & Haydon, P. G. (2017). Septal cholinergic neuromodulation tunes the astrocyte-dependent gating of hippocampal NMDA receptors to wakefulness. *Neuron*, 94(4), 840–854.e7. <https://doi.org/10.1016/j.neuron.2017.04.021>
- Papouin, T., Henneberger, C., Rusakov, D. A., & Oliet, S. H. R. (2017). Astroglial versus neuronal D-serine: Fact checking. *Trends in Neurosciences*, 40(9), 517–520. <https://doi.org/10.1016/j.tins.2017.05.007>
- Pascual, O., Casper, K. B., Kubera, C., Zhang, J., Revilla-Sanchez, R., Sul, J.-Y., Takano, H., Moss, S. J., McCarthy, K., & Haydon, P. G. (2005). Astrocytic purinergic signaling coordinates synaptic networks. *Science*, 310(5745), 113–116. <https://doi.org/10.1126/science.1116916>
- Paxinos, G., & Franklin, K. B. J. (2001). *The mouse brain in stereotaxic coordinates* (2nd ed.). Academic Press.
- Refaeli, R., Doron, A., Benmelech-Chovav, A., Groysman, M., Kreisel, T., Loewenstein, Y., & Goshen, I. (2021). Features of hippocampal astrocytic domains and their spatial relation to excitatory and inhibitory neurons. *Glia*, 69(10), 2378–2390. <https://doi.org/10.1002/glia.24044>
- Robin, L. M., da Cruz, J. F. O., Langlais, V. C., Martin-Fernandez, M., Metna-Laurent, M., Busquets-Garcia, A., Bellocchio, L., Soria-Gomez, E., Papouin, T., Varilh, M., Sherwood, M. W., Belluomo, I., Balcells, G., Matias, I., Bosier, B., Drago, F., Eeckhaut, A. V., Smolders, I., Georges, F., ... Marsicano, G. (2018). Astroglial CB1 receptors determine synaptic D-serine availability to enable recognition memory. *Neuron*, 98(5), 935–944.e5. <https://doi.org/10.1016/j.neuron.2018.04.034>
- Rusakov, D. A., Bard, L., Stewart, M. G., & Henneberger, C. (2014). Diversity of astroglial functions alludes to subcellular specialisation. *Trends in Neurosciences*, 37(4), 228–242. <https://doi.org/10.1016/j.tins.2014.02.008>
- Sakers, K., Lake, A. M., Khazanchi, R., Ouwenga, R., Vasek, M. J., Dani, A., & Dougherty, J. D. (2017). Astrocytes locally translate transcripts in their peripheral processes. *Proceedings of the National Academy of Sciences of the United States of America*, 114(19), E3830–E3838. <https://doi.org/10.1073/pnas.1617782114>
- Salmon, C. K., Syed, T. A., Kacerovsky, J. B., Alivodej, N., Schober, A. L., Sloan, T. F. W., Pratte, M. T., Rosen, M. P., Green, M., Chirgwin-Dasgupta, A., Mehta, S., Jilani, A., Wang, Y., Vali, H., Mandato, C. A., Siddiqi, K., & Murai, K. K. (2023). Organizing principles of astrocytic nanoarchitecture in the mouse cerebral cortex. *Current Biology*, 33(5), 957–972. <https://doi.org/10.1016/j.cub.2023.01.043>
- Santello, M., Toni, N., & Volterra, A. (2019). Astrocyte function from information processing to cognition and cognitive impairment. *Nature Neuroscience*, 22(2), Article 2. <https://doi.org/10.1038/s41593-018-0325-8>
- Sardinha, V. M., Guerra-Gomes, S., Caetano, I., Tavares, G., Martins, M., Reis, J. S., Correia, J. S., Teixeira-Castro, A., Pinto, L., Sousa, N., & Oliveira, J. F. (2017). Astrocytic signaling supports hippocampal-prefrontal theta synchronization and cognitive function. *Glia*, 65(12), 1944–1960. <https://doi.org/10.1002/glia.23205>
- Stogsdill, J. A., Ramirez, J., Liu, D., Kim, Y. H., Baldwin, K. T., Enustun, E., Ejikeme, T., Ji, R.-R., & Eroglu, C. (2017). Astrocytic neuroglins control astrocyte morphogenesis and synaptogenesis. *Nature*, 551(7679), 192–197. <https://doi.org/10.1038/nature24638>
- Sultan, S., Li, L., Moss, J., Petrelli, F., Cassé, F., Gebara, E., Lopatar, J., Pfrieger, F. W., Bezzi, P., Bischofberger, J., & Toni, N. (2015). Synaptic integration of adult-born hippocampal neurons is locally controlled by astrocytes. *Neuron*, 88(5), 957–972. <https://doi.org/10.1016/j.neuron.2015.10.037>
- Takata, N., Mishima, T., Hisatsune, C., Nagai, T., Ebisui, E., Mikoshiba, K., & Hirase, H. (2011). Astrocyte calcium signaling transforms cholinergic modulation to cortical plasticity in vivo. *The Journal of Neuroscience*, 31(49), 18155–18165. <https://doi.org/10.1523/JNEUROSCI.5289-11.2011>
- Tavares, G., Martins, M., Correia, J. S., Sardinha, V. M., Guerra-Gomes, S., Neves, S. P. d., Marques, F., Sousa, N., & Oliveira, J. F. (2017). Employing an open-source tool to assess astrocyte tridimensional structure. *Brain Structure and Function*, 222(4), 1989–1999. <https://doi.org/10.1007/s00429-016-1316-8>
- Torres-Ceja, B., & Olsen, M. L. (2022). A closer look at astrocyte morphology: Development, heterogeneity, and plasticity at astrocyte leaflets. *Current Opinion in Neurobiology*, 74, 102550. <https://doi.org/10.1016/j.conb.2022.102550>
- Wilhelmsson, U., Bushong, E. A., Price, D. L., Smarr, B. L., Phung, V., Terada, M., Ellisman, M. H., & Pekny, M. (2006). Redefining the concept of reactive astrocytes as cells that remain within their unique domains upon reaction to injury. *Proceedings of the National Academy of Sciences of the United States of America*, 103(46), 17513–17518. <https://doi.org/10.1073/pnas.0602841103>
- Wolosker, H., Balu, D. T., & Coyle, J. T. (2016). The rise and fall of the d-serine-mediated gliotransmission hypothesis. *Trends in Neurosciences*, 39(11), 712–721. <https://doi.org/10.1016/j.tins.2016.09.007>
- Xu, G., Wang, W., & Zhou, M. (2014). Spatial organization of NG2 glial cells and astrocytes in rat hippocampal CA1 region. *Hippocampus*, 24(4), 383–395. <https://doi.org/10.1002/hipo.22232>
- Yang, Y., Ge, W., Chen, Y., Zhang, Z., Shen, W., Wu, C., Poo, M., & Duan, S. (2003). Contribution of astrocytes to hippocampal long-term potentiation through release of d-serine. *Proceedings of the National Academy of Sciences of the United States of America*, 100(25), 15194–15199. <https://doi.org/10.1073/pnas.2431073100>
- Young, K. M., Mitsumori, T., Pringle, N., Grist, M., Kessaris, N., & Richardson, W. D. (2010). An Fgfr3-iCreERT2 transgenic mouse line for studies of neural stem cells and astrocytes. *Glia*, 58(8), 943–953. <https://doi.org/10.1002/glia.20976>
- Zehnder, T., Petrelli, F., Romanos, J., De Oliveira Figueiredo, E. C., Lewis, T. L., Déglon, N., Polleux, F., Santello, M., & Bezzi, P. (2021). Mitochondrial biogenesis in developing astrocytes regulates astrocyte maturation and synapse formation. *Cell Reports*, 35(2), 108952. <https://doi.org/10.1016/j.celrep.2021.108952>
- Zhang, Q., Pangrsič, T., Kreft, M., Kržan, M., Li, N., Sul, J.-Y., Halassa, M., Van Bockstaele, E., Zorec, R., & Haydon, P. G. (2004). Fusion-related release of glutamate from astrocytes. *Journal of Biological Chemistry*, 279(13), 12724–12733. <https://doi.org/10.1074/jbc.M312845200>
- Zhou, P., Zhang, Y., Ma, Q., Gu, F., Day, D. S., He, A., Zhou, B., Li, J., Stevens, S. M., Romo, D., & Pu, W. T. (2013). Interrogating translational efficiency and lineage-specific transcriptomes using ribosome affinity purification. *Proceedings of the National Academy of Sciences of the United States of America*, 110(38), 15395–15400. <https://doi.org/10.1073/pnas.1304124110>
- Zisis, E., Keller, D., Kanari, L., Arnaudon, A., Gevaert, M., Delemonet, T., Coste, B., Foni, A., Abdellah, M., Cali, C., Hess, K., Magistretti, P. J., Schürmann, F., & Markram, H. (2021). Digital reconstruction of the neuro-glia-vascular architecture. *Cerebral Cortex*, 31(12), 5686–5703. <https://doi.org/10.1093/cercor/bhab254>

SUPPORTING INFORMATION

Additional supporting information can be found online in the Supporting Information section at the end of this article.

How to cite this article: Viana, J. F., Machado, J. L., Abreu, D. S., Veiga, A., Barsanti, S., Tavares, G., Martins, M., Sardinha, V. M., Guerra-Gomes, S., Domingos, C., Pauletti, A., Wahis, J., Liu, C., Cali, C., Henneberger, C., Holt, M. G., & Oliveira, J. F. (2023). Astrocyte structural heterogeneity in the mouse hippocampus. *Glia*, 1–16. <https://doi.org/10.1002/glia.24362>